LBL--29736

DE91 005233

Sintering behavior of doped ZnO powders for high field varistors

Massimiliano Ghirlanda

(M.S. Thesis)

Department of Materials Science and Mineral Engineering

University of California at Berkeley

and

Center for Advanced Materials

Materials and Chemical Science Division

Lawrence Berkeley Laboratory

University of California

Berkeley, CA 94720

August, 1990

This work was supported by the Division of Materials Science Office of Basic Sciences of the Department of Energy, under Contract No. DE-AC03-76SF00098; and by the Electronic Ceramic Division, No. 1842, of Sandia National Laboratory, Albuquerque NM.

Table of Contents

1 Introduction

The sintering of ZnO varistor precursor powders, doped with Co, Mn and different concentrations of Bi and Al, is investigated and discussed in relation with sintering models.

One purpose of the present study is to provide information valuable for the fabrication of high field varistors. As the fundamental parameter of these electronic components is the breakdown voltage per unit of thickness, which is determined by the number of grain boundaries per linear dimension, the grain size and the sintered density are crucial variables, and the sintering is a central step in the manufacturing of such varistors.

Sintering experiments performed at constant heating rate in a loading dilatometer provide data on the densification and creep of the compacted powders (an original technique is used for the determination of the creep strain).

Another goal of the present study is to provide an experimental basis for the interpretation of the evolution of the ratio between densification rate and creep rate in terms of competition between densification and microstructure coarsening. This is accomplished by taking advantage of the variety of sintering behaviors that takes place in the system ZnO-Bi-Al: the comparison of these behaviors allows us to correlate the macroscopic sintering parameters to the evolution of the microstructure.

It results that, while in non-doped powders densification and coarsening develop in a balanced way, resulting in the constancy of the ratio between densification rate and creep rate, the effect of the dopants on the sintering kinetics alters such a balance, leading this ratio to vary.

An expression for the densification strain rate, derived within the frame of a model devised by Swinkels and Ashby [1980] in which the densification is controlled by two processes in series, provides a new insight into the interplay between densification and coarsening, as it shows that in certain circumstances the kinetic mechanism governing the coarsening may control the densification as well.

2 Background

2.1 Sintering theory overview

Many theories of sintering have been devised in the last few decades. In this paragraph an overview of the basic concepts common to most of these theories is presented, focusing on the importance of the interconnection between densification and microstructure coarsening. Several review articles are available for a detailed description of the various theories [Burke and Rosolowsky 1976, Coble and Cannon 1978, Johnson 1979, Kuczynski 1985, German 1985 on liquid phase sintering].

The common ground of all sintering theories is the identification of the driving force for sintering with the tendency of a porous compact to lower its free energy connected with solid-vapor interfaces. This is accomplished in two ways:

- By reduction of the total surface of the grains as a consequence of their growth and coalescence (microstructure coarsening).

- By substitution of grain-pore interfaces with grain-grain boundaries (having lower energy), as a consequence of pore shrinkage (densification).

Densification and microstructure coarsening are the two fundamental phenomena occurring during sintering. The sintering behavior of most systems can be interpreted in terms of the competitive effect and interaction of the two phenomena.

2.1.1 Coarsening

Microstructure coarsening occurs by the Ostwald ripening mechanism, for which inhomogeneous particle and pore size distributions provide the driving force. Surface diffusion and evaporation-condensation are the typical mechanisms for mass transport in solid phase coarsening, while in the presence of an intergranular liquid phase, a solution-precipitation process is often dominant. A coarse microstructure develops as large grains and pores grow further at the expenses of smaller ones, which eventually disappear allowing the scale of the structure to increase.

The classical coarsening theory was developed independently by Lifshitz and Slevotz [1961] and by Wagner [1961]. Models of the coarsening of the microstructure during sintering of porous systems have been proposed by several authors, usually in terms of topological requirements for space filling and evolution of the grain size. Recently, significant contribution has been brought by techniques of computer simulation. Good reviews are by Hillert [1965], Brook [1976] and Atkinson [1988].

2.1.2 Densification

Densification occurs typically by grain boundary or lattice diffusion. The driving force for densification has been the object of extensive study. Typical approaches consider local geometrical parameters, such as pore curvature and dihedral angle, grain size, neck radius, pore coordination number and interpore spacing [Beere 1975, Jagota *et al* 1988, De Jonghe *et al* 1989, Cannon and Carter 1989]. Other studies relate the densification to the pore/particle size distribution [Whittemore and Varela 1979, Patterson *et al* 1985], or to the structural evolution of the pore network [Barrett and Yust 1967, DeHoff 1984, Rhines and DeHoff 1984]. The role of the surface energy in relation to anisotropy and temperature gradients has also been investigated [Searcy 1985 and 1987, Beruto *et al* 1989]. To a first

approximation, however, the densification driving force can be considered proportional to the mean pore curvature [De Jonghe *et al* 1989].

2.1.3 Interplay of densification and coarsening

As densification develops by pore shrinking, its effect on the pore size is the opposite of that produced by coarsening. Since the pore curvature corresponds roughly to the inverse of the pore size, densification appears as a self-enhancing phenomenon, whose effects increase its own driving force. On the other hand coarsening is expected to affect negatively the densification and its own further development as well, not only because the scale of the microstructure is inversely proportional to the driving force for both phenomena, but also because a coarse microstructure corresponds to a large diffusional path and thus to slow kinetics.

It is evident that densification and coarsening are strictly related. A study of the sintering behavior of a system must explore the interplay of these two phenomena.

2.2 An experimental way to determine the sintering driving force

In recent years De Jonghe and Rahaman [1984] have introduced an experimental technique to determine the overall driving force for densification from measurements of densification and creep. Such a driving force, called the *sintering stress*, is defined as the equivalent external mechanical stress that would give rise to the same densification strain rate as the internal driving force.

Since this technique is used in the present study, its theoretical foundations will be reviewed.

The densification strain of a compact is defined as follows:

$$\varepsilon_d = \frac{1}{3} \ln\left(\frac{\rho}{\rho_o}\right) \qquad \text{Eqn. 2.1}$$

where ρ and ρ_o are the actual and the initial density of the compact.

The creep strain occurring in a compact under applied uniaxial load is defined as:

$$\varepsilon_c = \varepsilon_z - \varepsilon_d \qquad \text{Eqn. 2.2}$$

where ε_z is the axial strain = $\ln (z/z_o)$; with z and z_o being the actual and initial dimension of the compact along the axis of the applied load.

The densification strain rate is expressed by many authors [Frenkel 1945, Coble 1961, De Jonghe and Rahaman 1984 and 1988] by means of the following generic equation:

$$\dot{\varepsilon}_d = \frac{1}{\eta_d}(\Sigma + \sigma_h) \qquad \text{Eqn. 2.3}$$

Σ is the sintering stress , σ_h is the externally applied hydrostatic stress (when uniaxial stress σ is applied, $\sigma_h = \frac{1}{3}\sigma$ [Chu *et al.* 1989]). η_d is the *densification viscosity*, which contains the various kinetic parameters such as the diffusion coefficient, temperature and diffusion length.

The definition of Σ leads to the following relation:

$$\sigma_{gb} = \Sigma \phi \qquad \text{Eqn. 2.4}$$

where σ_{gb} is the effective densification stress acting on the grain boundaries, and ϕ is the *stress intensification factor* = total area / grain boundary area.

Similarly, the creep strain rate can be expressed in the following form:

$$\dot{\varepsilon}_c = \frac{1}{\eta_c}(\sigma)^s \qquad \text{Eqn. 2.5}$$

Where now η_c is the *creep viscosity*. The stress exponent s depends on the creep mechanism and can range from 1 to 5 [Brook 1982]. Under conditions of low applied stress, creep occurs by diffusion and s equals 1.

To express η_d and η_c in terms of physical parameters we need to adopt a model for the transport of matter in the compact. Rigorous models are available for ideal conditions of uniform particle size and packing distribution. Various geometrical configurations can be considered. At least two different configurations (spherical particles connected by a neck, in simple cubic arrangement [Chu 1990], which ideally describes the early sintering stages, and pores at the grain boundary corners in cylindrical geometry, corresponding to later stages of sintering [De Jonghe and Rahaman 1988]) lead to the same form of equation for η_d:

$$\eta_d \propto A_d(T)\,\frac{G^n}{\phi^{\frac{n+1}{2}}} \qquad \text{Eqn. 2.6}$$

Where A_d is a temperature-dependent term, G is the grain size, ϕ is the stress intensification factor, and n is an exponent which depends on the prevailing diffusion mechanism: n = 3 for grain boundary diffusion and n = 2 for bulk diffusion.

Under the effect of a low applied stress the diffusion mechanisms adopted by the atoms to migrate from grain boundaries in compression to grain boundaries in tension (or by the vacancies to travel the opposite path), can be assumed to be the same as those generating densification [De Jonghe and Rahaman 1988]; therefore:

$$\eta_c \propto A_c(T) \frac{G^n}{\phi^{\frac{n+1}{2}}} \qquad \text{Eqn. 2.7}$$

Now, since both A_d and A_c depend on the temperature in the same way[1]:

$$\frac{\eta_c}{\eta_d} = \text{constant} = K \qquad \text{Eqn. 2.8}$$

Combining Eqns. 2.3, 2.4 and 2.8, it follows that the ratio between densification and creep rate is linearly dependent on the sintering stress Σ, as expressed by the equation:

$$\frac{\dot{\varepsilon}_d}{\dot{\varepsilon}_c} = K\left(\frac{\Sigma}{\sigma} + \frac{1}{3}\right) \qquad \text{Eqn. 2.9}$$

The validity of Eqn. 2.8 has been experimentally confirmed for some specific systems [Rahaman at al 1988, De Jonghe and Srikanth 1988]. An indication of the reliability of the proportionality between the rate ratio and the sintering stress comes also from the observation that in a number of systems (ZnO, CdO, MgO, MgO-Bi_2O_3, $YBa_2Cu_3O_x$, glass) the ratio $\dot{\varepsilon}_d/\dot{\varepsilon}_c$ is constant from the onset of the densification to the final stages of sintering [Chu *et al* 1989]. Because a compensating effect between the viscosity ratio K and the sintering stress is unlikely considering the variety of systems concerned, both terms are argued to be constant.

---

[1] $A_d, A_c \propto \frac{\kappa T}{D(T)}$ where κ is the Boltzman constant, T the absolute temperature, D(T) the diffusion coefficient

2.3 Sintering of ZnO ceramics

2.3.1 Pure ZnO

A number of investigators have studied the sintering of pure ZnO powder compacts, mainly for the purpose of determining the kinetic processes. Studies based on the activation energy measurement at high sintering temperatures ($900^{o}C$-$1400^{o}C$), by Gupta and Coble [1968], Dutta and Spriggs [1968] and recently Senda and Bradt [1990], indicate that at these temperatures Zn^{2+} lattice diffusion is probably the rate limiting process for densification as well as for coarsening. Analogous studies, on the other hand, indicate that during the early stages of sintering [Norris and Parravano 1963] and at relatively low temperatures ($600^{o}C$-$900^{o}C$) [Komatsu *et al* 1969, Whittemore and Varela 1981, Senos *et al* 1987?] surface diffusion and grain boundary diffusion are respectively responsible for coarsening and densification. Whittemore and Powell [1983] have addressed the issues of the effects of oxygen pressure and water vapor on the sintering of ZnO.

Rahaman and De Jonghe [1987] have investigated the sintering of ZnO compacts under an applied stress of 0.25 psi; reporting a constant value of the ratio $\dot{\varepsilon}_d / \dot{\varepsilon}_c$ in the density range 0.55% - 0.85%.

2.3.2 The Bi_2O_3 - ZnO system

The sintering of Bi_2O_3 - ZnO varistor precursor powders has been investigated by several authors, although most of the studies are mainly concerned with the effects of sintering parameters on the electrical properties of the varistors. Since commercial varistors often contain various other dopants that, like Bi_2O_3, affect the microstructure evolution (such as Sb_2O_3 and Cr_2O_3), in most of the cases the effect of Bi_2O_3 can hardly be isolated

from the others'; moreover the analysis can be further complicated by the formation of secondary phases, such as spinel and pyrochlore.

In general Bi_2O_3 doping (above a concentration of 0.1 mol% [Kim *et al* 1989]) is reported to accelerate densification and enhance grain growth and microstructure inhomogeneity, as a consequence of the formation of a liquid bismuth-rich intergranular phase in which the ZnO grains are soluble [Wong 1980, Sung *et al* 1987, Kim *et al* 1989, Mantas and Baptista 1989]. The eutectic temperature for the system ZnO-Bi_2O_3 is 740°C [Safronov *et al* 1971]. Abnormal grain growth and residual intragranular porosity are often reported.

In liquid phase sintering the transport of matter occurs typically by a solution-precipitation process [German 1985], in which, for ZnO-Bi_2O_3 ceramics, the limiting step is probably the phase boundary reaction of the ZnO with the Bi-rich liquid, rather than the diffusion of ZnO within the liquid phase [Senda and Bradt 1990].

Since Bi_2O_3 is essentially insoluble in ZnO at ambient temperatures, during cooling it segregates in second phases either at grain boundaries or at grain boundary junctions [Clarke 1977, Levinson and Philipp 1978]. The wetting of the ZnO grains by the liquid phase has been reported by Gambino *et al* [1989] to be dependent on the temperature, and this fact has been related to the temperature dependence of the ZnO concentration in the second phase.

2.3.3 The effect of the aluminum

Less literature is available on the sintering of Al-doped ZnO ceramics. Carlson and Gupta [1982] and Kimball and Dought [1987] have reported on the inhibiting effect of aluminum on the grain growth of doped ZnO varistors; while Komatsu *et al* [1968] have observed that aluminum retards the densification. These effects may be consequences of a

depletion of the interstitial Zn^{2+} concentration due to the substitution of Zn by Al in the crystal lattice.

Carlson and Gupta [1982] and Takemura *et al* [1982] were able to determine the distribution of the aluminum within the microstructure of commercial varistors. High concentrations of Al were found in an Sb-rich spinel phase, but no difference in Al concentration could be detected between the ZnO grains and the Bi-rich phase (due perhaps to an insufficient detection limit).

3 Experiments

3.1 The six powders

Six different types of varistor precursor powder, provided by Sandia National Laboratory, were used in the experiments. The composition of the powders was the following[2]:

O : ZnO 99.5 mol% , CoO 0.25 mol% , MnO 0.25 mol%

A : same as **O** + Al 340 ppm

A2 : same as **O** + Al 142 ppm

B : ZnO 98.94 mol% , CoO 0.25 mol% , MnO 0.25 mol% , Bi_2O_3 0.56 mol%

AB : same as **B** + Al 340 ppm

AB2: same as **B** + Al 142 ppm

The powder preparation method was tailored to produce varistors with the additive distribution characteristics of commercial varistors, and with a submicron grain size required for high-voltage application[3]. The Zn, Co, Mn and, when present, Al were coprecipitated as hydrous oxides that were immediately converted to oxalates and then calcined to produce an oxide mixture. In bismuth-doped powders, Bi was precipitated on the surface of the oxides by a localized hydrolysis reaction. The preparation process is

[2] In this study a bold capital character will identify one of the six types of doped ZnO powder.

[3] Because the breakdown voltage of a varistor is determined by the number of grain boundaries per unit of thickness (each of them contribute with a voltage drop in the order of 2-4 V), grain size control is a fundamental aspect in the sintering of this type of varistors.

reported in detail in works by Dosch *et al* [1985], Kimball and Doughty [1987], Gardner and Lockwood [1988] and Lockwood and Gardner [1988].

3.2 Compaction

Uniaxial compaction of the powders was performed in a die at ~ 10,000 psi, to obtain pellets of 6.42 mm in diameter by ~5.5 mm in length. The resulting green density of each type of powders, averaged over several pellets, is reported in table 1. A maximum difference of 0.5% in the relative density was allowed between green pellets of the same powder.

3.3 Sintering

Using a loading dilatometer [De Jonghe and Rahaman 1984], sintering was performed at the constant heating rate of 4^{o}C/min, between 300^{o}C and 1000^{o}C. For each type of powder at least 2 pellets were sintered without applied load and at least 2 under an applied load of 6 N (corresponding to an initial stress on the compact of 0.185 MPa) for powder **O, B, AB** and **AB2**; of 8 N (= 0.247 MPa) for **A** and **A2** (for the purpose of obtaining a higher creep). The load was applied as the temperature reached 500^{o}C and mantained until the end of the experiment. Mass and dimensions of the pellets were measured before and after sintering, and the final densities were verified using Archimedes' method. 6 sets of sintering runs where so performed.

In addition, for all powders a number of sintering runs (with and without load) were interrupted at lower temperatures to measure the dimensions of the pellets and to observe their microstructures at intermediate stages of sintering. A few sintering runs were performed using pellets with a different green density, for the purpose of determining the role of this parameter on the sintering behavior.

3.4 Microscopy

Fracture surfaces and polished and etched sections of pellets sintered at various temperateres were examined using the SEM. Two etching methods were used: chemical etching was performed using a dilute solution of acetic acid; thermal etching (~1 minute at 1,000^{o}C), however, was more effective.

The mean grain size of a sintered compact was calculated as follows from at least two micrographs taken from different regions of the compact's section: for loosily sintered compacts, between 50 and 100 grains were measured from each micrograph of their fracture surface. For denser compacts, polished and etched sections were considered: grain sizes were measured by counting the number of grain boundaries intersected by straight lines of known length (about 5 straight lines were drawn on each micrograph). The average grain size was taken as 1.5 times the average inrcept length.

4 Manipulation of the Data

4.1 Axial strain

Each sintering experiment provided two sets of data: the sintering temperature T measured by a thermocouple in the proximity of the sample, and the sample axial shrinkage Δz, linearly proportional to the voltage output of the loading dilatometer. T' and Δz were recorded at short intervals of time during sintering, so that they could be plotted as function of the sintering time t.

The axial strain of a sample during sintering was calculated as follows:

$$\varepsilon_z = \ln\left(1 + \frac{\Delta z}{z_0}\right) \qquad \text{Eqn. 4.1}$$

where z_0 is the initial axial dimension.

The experiments were performed at constant heating rate α, so that:

$$\Delta T = \alpha\, t \qquad \text{Eqn. 4.2}$$

Therefore ε_z could also be plotted versus T.

For each type of powder, two different curves of ε_z vs. T were obtained from the average of several sintering runs in each of the two following conditions: free sintering and sintering under applied stress. Aside from the applied stress and within the limits of the experimental error, the two sets of sintering runs were performed under identical conditions of green density, sintering temperature range and heating rate.

4.2 Densification strain

By measuring the diameter of the sintered samples, their final radial strain $\varepsilon_{r.fin}$ was calculated from

$$\varepsilon_r = \ln\left(\frac{r}{r_0}\right) \qquad \text{Eqn. 4.3}$$

with r and r_0 equal to the actual and initial radius of the sample.

Since:

$$3\,\varepsilon_d = \varepsilon_z + 2\,\varepsilon_r \qquad \text{Eqn. 4.4}$$

the final densification strain $\varepsilon_{d.fin}$ could be calculated from the equation:

$$\varepsilon_{d.fin} = \frac{1}{3}(\varepsilon_{z.fin} + 2\,\varepsilon_{r.fin}) \qquad \text{Eqn. 4.5}$$

For non loaded samples $\varepsilon_{z.fin}$ and $\varepsilon_{r.fin}$ were verified to coincide to within +/- 3%. Consequently, from Eqn.4.4, for each type of powder the ε_z curve obtained from free sintering was assumed to represent the densification strain during sintering (ε_d).

The densification strain rate $\dot{\varepsilon}_d$ was obtained from the curve of ε_d vs. T:

$$\dot{\varepsilon}_d = \frac{d(\varepsilon_d)}{dT}\,\alpha \qquad \text{Eqn. 4.6}$$

4.3 The modified creep strain

Combining Eqn 2.2 with Eqn. 4.4, the creep strain ε_c of a loaded sample can be determined from the relation:

$$\varepsilon_c = \frac{2}{3}(\varepsilon_z - \varepsilon_r) \qquad \text{Eqn. 4.7}$$

The usual way to evaluate the creep strain during sintering is thus by measuring both the axial and the radial strain at various stages of the sintering. Unfortunately ε_r is available only if we stop the sintering to measure the diameter of the sample, with the consequence of errors due to transients in temperature and in load. Furthermore, a large number of sintering runs under identical conditions are necessary to plot a reliable curve of ε_c, expecially since such a curve must be determined with great accuracy as it has to be differentiated to provide the creep rate.

A simpler and possibly more accurate procedure is available: A *modified creep strain* ε_{cm} is defined as follows,

$$\varepsilon_{cm} = \varepsilon_z(\sigma) - \varepsilon_d(0) \qquad \text{Eqn. 4.8}$$

where $\varepsilon_z(\sigma)$ is the axial strain characteristic of a type of powder sintered under applied stress σ, and $\varepsilon_d(0)$ is the corresponding densification strain measured under identical conditions, but without applied stress. The evolution of the modified creep strain is therefore represented by a curve versus the sintering temperature, resulting from the difference between the two axial strain curves described earlier. It should be noted that the modified creep strain is associated with the sintering of a type of powder under given conditions, but, unlike the true creep strain, is not measurable from a single sintered pellet.

From the comparison of Eqn. 4.8 with Eqn. 2.2 it is evident that the modified creep strain coincides with the creep strain only if the applied stress does not affect the densification, as expressed by:

$$\varepsilon_{cm} = \varepsilon_c + \left(\varepsilon_d(\sigma) - \varepsilon_d(0)\right) \qquad \text{Eqn. 4.9}$$

Direct measurements of the sample's dimensions were taken at various stages of the sintering to evaluate the effect of the applied stress on the density. Since no appreciable

effect was detected, and since the densification strain is not expected to change considerably in response to a very small variation of the density, the modified creep strain was assumed to express the true creep strain.

The curve of the creep strain rate was then obtained by differentiation, in a way analogous to Eqn. 4.6.

The following correction to the creep rate was applied to account for the variation of the actual applied stress as a consequence of the reduction of the sample's apparent cross sectional area during densification:

$$\dot{\varepsilon}_c(\sigma_o) = \dot{\varepsilon}_c(\sigma) \exp(\varepsilon_c - 2\varepsilon_d) \qquad \text{Eqn. 4.10}$$

where $\dot{\varepsilon}_c(\sigma_o)$ is the creep rate due to a constant applied stress σ_o equal to the initial value of σ.

Finally, the ratio $\frac{\dot{\varepsilon}_d}{\dot{\varepsilon}_c}$ was calculated and plotted versus T.

4.4 Plotting versus density

The curve of the density vs. temperature for each powder was obtained from:

$$\rho = \rho_o \exp(3\,\varepsilon_d) \qquad \text{Eqn. 4.11}$$

with ρ_o equal to the green density.

As the density is a monotonic function of the temperature, all the sintering variables (ε_d, $\dot{\varepsilon}_d$, $\dot{\varepsilon}_c$, $\frac{\dot{\varepsilon}_d}{\dot{\varepsilon}_c}$) could be plotted versus the density as well.

5 Results and analysis

5.1 Tables and figures

An overview of the experimental results relative to the densification and creep from the sintering of the six types of powders is presented in table 1, while in table 2 the mean grain size of the various powders is reported for several sintering temperatures. Figs. 1 - 5 show SEM micrographs of the compacts microstructure taken at various stages of the sintering. In Figs. 6 - 8 grain size data are plotted vs. temperature and densification strain. In Figs. 9 - 13 densification and creep parameters are plotted vs. the temperature, while in Figs. 14 and 15 some of them are plotted vs. the density. The effect of a variation in the green density on the densification rate is shown for one type of powder in fig. 16.

5.2 Microstructure

The six powders show a similar green microstructure, characterized by particle agglomerations of the size of several microns (fig. 1a). The spherical particles are nearly monosized with a mean diameter of about 60 nm (Fig. 1c,d) (The Al-doped powders, **A** and **A2**[4], are somewhat larger; see the data on the grain size in table 2).

In spite of the initial similarity the evolution of the microstructure during sintering is extremely diversified in the various powders, as shown in Figs. 6, 7 and 8.

By comparing the grain growth in **A** and **A2** with that in **O**, it results that during the first half of the sintering Al-doping hinders the grain growth to an extent depending on the content of aluminum. Eventually the coarsening of **A** and **A2** appears to take place at

[4]Recall that bold capital characters identify types of powders

higher rates. In these powders the porosity becomes closed between 850^{o}C and 900^{o}C, when the pores have the size of few hundreds nanometres (Figs.4a,b).

In **B**, substantial grain growth is observed already at 710^{o}C (Fig, 2d). at 735^{o}C small particles (< 50 nm) probably composed of a Bi-rich second phase are formed next to the large faceted ZnO grains (Fig.3d). The grain growth is further amplified and associated with a loss of homogeneity, as a liquid phase forms at the boundary junctions and gradually decreases its contact angle with the grains (Fig. 4d). Pore coalescence, abnormal grain growth and intragranular porosity are observed at the late stages of sintering (Fig.5a,b), unlike in any other type of powder. Small micropores are found within the intergranular phase of the sintered compacts (possibly formed during the cooling process).

A competition between the effects of bismuth and aluminum seems to take place in **AB** and **AB2**, where the formation of a liquid phase and its development (i.e. the lowering of the contact angle) is retarded to an extent dependent upon the aluminum concentration.

The evolution of the microstructure in **AB2** follows more closely that of **B** (expecially during the first part of the sintering), and the presence of a liquid phase having low contact angle with the grains is observed at 800^{o}C (Fig.4e).

The microstructure of **AB** is still very fine and homogeneous at 730^{o}C, where the particles appear to be coated by a non-crystalline phase that smooths their shape (Fig.2f). Small second phase particles are observed only at 790^{o}C, when considerable grain growth had already ocurred. The development of a liquid phase, associated with extensive grain growth, continues throughout the late stages of sintering.

5.3 Densification and creep

Direct measurements of the compact densities during sintering showed that increments typically lower than 3% were produced by the applied load. Such an effect was considered small enough to allow us to use the technique described in section 4.3 for the determination of the creep strain.

In relation to their densification and creep behavior during sintering, the six powders can be subdivided into two groups: powders where no liquid phase occurs (**O, A** and **A2**), and powders for which liquid phase sintering is observed (**B**, **AB** and **AB2**).

5.3.1 Powders O, A and A2

The densification of the three powders (Figs. 9a and 11a) show a similar trend, although the aluminum clearly affects negatively the rate of the process to an extent depending on its concentration. As a result, while **O** completes its densification at ~980^{o}C, **A** and **A2** are still densifying at 1000^{o}C (the density of **A** stabilizes only at ~1050^{o}C).

The inhibiting effect of the aluminum is particularly evident on the creep (Figs. 10a and 12a). The curve of $\dot{\varepsilon}_c$ is not similar in the three powders as that of $\dot{\varepsilon}_d$: rather than following a smooth path as in **O**, in **A** $\dot{\varepsilon}_c$ stops rising quite abruptly around 690^{o}C, in **A2** at ~750^{o}C, and then remains almost constant until ~950^{o}C. This trend is even more evident in the graph of $\dot{\varepsilon}_c$ vs. ρ, where, in the density range 55% - 90%, $\dot{\varepsilon}_c$ appears constant in **A2** and slightly decreasing in **A** (Fig. 14a).

5.3.2 powders B, AB and AB2

As was the case for coarsening, doping with Bi_2O_3 enhances the rate of densification and creep dramatically. The addition of aluminum counteracts the influence of bismuth in **AB** and **AB2**, causing a reduction in the peak values of $\dot{\varepsilon}_d$ and $\dot{\varepsilon}_c$ scaling with its concentration (and in **AB** determining a delay of such peak) (Figs. 11b, 12b and 14b).

In all three powders the rise of $\dot{\varepsilon}_d$ and $\dot{\varepsilon}_c$ occur in correspondence with a sharp increase of the grain growth (shown in Fig. 7), that is always before evidence of the formation of a liquid phase, and, for **B** and **AB2,** below the eutectic temperature for the system $ZnO\text{-}Bi_2O_3$ (740°C)[2].

Although densification and creep strain are slower for **AB** and **AB2**, their final values are actually higher than those for **B**. The lower final density of **B** is associated with the residual intragranular porosity and with porosity embedded in the second phase. The difference in the final creep strain instead, is due to a steady increase of ε_c in **AB** and **AB2**, that continues after the end of the densification process.

5.4 Green density and densification

The effect of a variation of the green density on the curve of the densification has been evaluated for **AB**: an increment of 1% in ρ_o shifts the position of the peak of $\dot{\varepsilon}_d$ downward by 10°C, while the height of such peak appears unmodified (Fig.16).

[2]The phase diagram for the ternary system $ZnO\text{-}Bi_2O_3\text{-}Al_2O_3$ could not be found in the literature.

5.5 The ratio between densification rate and creep rate.

The evolution of the ratio between densification rate and creep rate for the six types of powder is here considered in relation to coarsening and densification. Although the coarsening phenomenon is not fully expressed by one single parameter, we have to base our analysis on the only data readily available from microscopy: the mean grain size .

From the comparison of the various curves of $(\dot{\varepsilon}_d/\dot{\varepsilon}_c)$ vs. T in Fig. 13, with the plots of G vs. T in Fig.6, we observe that where the ratio of rates increases, the slope of the curve of the grain size is lower with respect to the same curve for powder **O**. This is evident in **A** and **A2** up to ~850^{o}C, in **AB** before ~730^{o}C and in **AB2** before 710^{o}C. Conversely, a decreasing trend for $(\dot{\varepsilon}_d/\dot{\varepsilon}_c)$ corresponds to relatively high slope for G vs. T in **A** after 850^{o}C, in **AB** and **AB2** after 730^{o}C, and in **B** throughout the entire sintering process.

A better choice for the analysis of the coarsening dynamics is the grain growth parameter, defined as follow:

$$\varepsilon_g = \ln (G/Go) \qquad \text{Eqn. 5.1}$$

If ε_g is plotted versus the temperature the (inverse) relationship between grain growth (i.e. coarsening) and the trend of $(\dot{\varepsilon}_d/\dot{\varepsilon}_c)$ is even more evident (Fig. 7).

The plot of ε_g vs. ε_d allows us to visualize the competition between densification and coarsening (Fig. 8). It results that in powder **O** the constancy of $(\dot{\varepsilon}_d/\dot{\varepsilon}_c)$ corresponds to an approximatively linear relation between densification and grain growth, expressed by $\varepsilon_g = \kappa\, \varepsilon_d$, with $\kappa \sim 9$. In the other powders a relatively higher slope of ε_g vs. ε_d corresponds to a decrease of $(\dot{\varepsilon}_d/\dot{\varepsilon}_c)$, and vice versa.

As the microstructure data of this study are rather limited, any attempt to determine with further accuracy a quantitative relation between ε_g, ε_d and $(\dot{\varepsilon}_d/\dot{\varepsilon}_c)$, would probably be inappropriate.

6 Discussion

An interesting result of the present study is in the different behavior of the ratio between densification rate and creep rate during the sintering of the various powders.

In the following section a clue for the interpretation of these behaviors is obtained by deriving the equation for the densification rate within the frame of a model devised by Swinkels and Ashby [1980]. According with this model, the rate of the densification by grain boundary diffusion can actually be limited, under certain circumstances, by the redistribution process of the matter within the pore surface, which is driven by a local potential gradient associated with differences in the pore curvature near the neck boundary.

6.1 Densification by two mechanims in series.

In the Swinkels and Ashby approach grain boundary diffusion and surface redistribution are two mechanisms in series, controlling the rate of densification. Assuming a quasi-steady state condition the rate of matter transport out of the grain boundary is equal to the rate of redistribution; this condition can be written in a form that relates the densification strain rate to the driving forces and kinetics of the two mechanisms. When no external stress is applied:

$$\dot{\varepsilon}_d = \frac{\Delta\Sigma_{gb}}{\eta_{gb}} = \frac{\Delta\Sigma_s}{\eta_s} \qquad \text{Eqn. 6.1}$$

Where $\Delta\Sigma_{gb}$ and $\Delta\Sigma_s$ are the driving force for transport of matter respectively by grain boundary diffusion and surface redistribution. Correspondingly, η_{gb} and η_s are the viscosities for these processes, containing the proper geometrical parameters and diffusion coefficients.

Since $\Delta\Sigma_{gb}$ and $\Delta\Sigma_s$ are two driving forces in series, their sum provides the total internal driving force for densification. If $\Delta\Sigma_{gb}$ and $\Delta\Sigma_s$ are defined as corresponding to externally applied stresses, the internal densification driving force coincides with the sintering stress Σ defined in section 2.2[1]:

$$\Delta\Sigma_{gb} + \Delta\Sigma_s = \Sigma \qquad \text{Eqn. 6.2}$$

Σ is determined by the (maximum) curvature of the pore surface away from the neck boundary, K_p, divided by the stress intensification factor ϕ (see De Jonghe *et al* [1989]).

$$\Sigma = \gamma \frac{K_p}{\phi} \qquad \text{Eqn. 6.3}$$

Similarly, $\Delta\Sigma_{gb}$ and $\Delta\Sigma_s$ can be defined as follows:

$$\Delta\Sigma_{gb} = \gamma \frac{K_n}{\phi} \qquad \text{Eqn. 6.4}$$

$$\Delta\Sigma_s = \gamma \frac{K_p - K_n}{\phi} \qquad \text{Eqn. 6.5}$$

where K_n is the pore curvature at the neck boundary (see Swinkels and Ashby [1980]).

From Eqns. 6.1 and 6.2 we can write:

$$\dot{\varepsilon}_d = \frac{\Sigma}{\eta_d} \qquad \text{Eqn. 6.6}$$

where η_d is the total densification viscosity given by:

$$\eta_d = \eta_{gb} + \eta_s \qquad \text{Eqn. 6.7}$$

[1]Consequently η_{gb} is defined by Eqn. 2.6 (with n=3). An expression for η_s is derived in the Appendix.

When an external uniaxial stress σ is applied, it contributes to the stress acting on the grain boundary, and Eqn. 6.1 becomes:

$$\dot{\varepsilon}_d = \frac{\Delta\Sigma_{gb} + \frac{\sigma}{3}}{\eta_{gb}} = \frac{\Delta\Sigma_s}{\eta_s} \qquad \text{Eqn. 6.8}$$

or:

$$\dot{\varepsilon}_d = \frac{\Sigma + \frac{\sigma}{3}}{\eta_d} \qquad \text{Eqn. 6.9}$$

6.1.1 A new expression for the ratio between densification rate and creep rate.

Consider the creep strain rate expressed as follows:

$$\dot{\varepsilon}_c = \frac{\sigma}{\eta_c} \qquad \text{Eqn. 6.10}$$

where σ is the applied uniaxial stress and η_c is the creep viscosity as in Eqn. 2.7.

Combining Eqns. 6.9, 6.10, we obtain:

$$\frac{\dot{\varepsilon}_d}{\dot{\varepsilon}_c} = \frac{\eta_c}{\eta_d}\left(\frac{\Sigma}{\sigma} + \frac{1}{3}\right) \qquad \text{Eqn. 6.11}$$

Then, substituting Eqns. 6.7 and 2.8 in Eqn. 6.11:

$$\frac{\dot{\varepsilon}_d}{\dot{\varepsilon}_c} = K\frac{\eta_{gb}}{\eta_{gb} + \eta_s}\left(\frac{\Sigma}{\sigma} + \frac{1}{3}\right) \qquad \text{Eqn. 6.12}$$

If the redistribution step is negligible, as usually assumed, Eqn. 6.12 reduces to Eqn. 2.9, describing the situation in which densification and creep are governed by the

same kinetics, so that the ratio between densification rate and creep rate is proportional only to the sintering stress.

On the other hand, if the redistribution step is not negligible, $(\dot{\varepsilon}_d/\dot{\varepsilon}_c)$ depends also on the kinetic term $\left(\frac{\eta_{gb}}{\eta_{gb}+\eta_s}\right)$.

The generic form of the viscosities is:

$$\eta = F\frac{kT}{D(T)} \qquad \text{Eqn. 6.13}$$

where F is a generic function containing the geometrical terms, k is the Boltzman constant, T the absolute temperature and D(T) is the diffusion coefficient correspondent to the transport mechanism.

Since surface redistribution and coarsening exploit the same kinetic mechanisms, η_s can be related to a coarsening viscosity. We may notice that, if a situation of equilibrium between densification and coarsening is initially present in the system, according to Eqn. 6.12 such equilibrium tends to be preserved despite variations of the kinetic terms. As a matter of fact, a variation of the ratio of the viscosity $\left(\frac{\eta_{gb}}{\eta_{gb}+\eta_s}\right)$ would alter the terms of the equilibrium in a way that the consequent modification of Σ would tend to compensate the effect of such variation upon $(\dot{\varepsilon}_d/\dot{\varepsilon}_c)$. For example: if η_s increases the coarsening kinetic slows down, while the densification rate is less affected because of its dependence on η_{gb} (from Eqn. 6.7). As a result coarsening loses ground relative to the densification, the pore tends to shrink and $\frac{Kp}{\phi}$, i.e. Σ, tends to increase, counteracting the decrease of the ratio of the viscosity.

The contribution of the kinetic term in Eqn. 6.12 can be, however, completely different if the densification starts from a situation of non-equilibrium, such as the one that arises if the kinetic mechanisms for densification and coarsening are activated at different times, as shown in the following section.

6.1.2 Kinetic transient during non-isothermal sintering.

To complete the analysis of the ratio between densification and creep rate in the various cases we now need to consider Eqn. 6.12 in a more dynamic perspective in relation to the evolution of the viscosities during non isothermal sintering (for simplicity constant heating rate sintering will be considered).

As diffusion is virtually absent at ambient temperature, the initial value of the viscosities η_s and η_{gb} is nearly infinite and $(\dot{\varepsilon}_d/\dot{\varepsilon}_c)$, from Eqn. 6.12, is indeterminate. During the first stage of constant heating rate sintering, the viscosities drop several orders of magnitude in relation to the increase of the diffusion coefficients: these are related to the concentration of point defects and thus depend on the temperature through the Arrhenius equation:

$$D = D^o \exp(-\frac{Q}{kT}) \qquad \text{Eqn. 6.14}$$

where D^o is a constant which includes the entropy and kinetic terms, and Q the activation energy of the process.

A dynamic situation, characterized by considerable variation of the value of $(\dot{\varepsilon}_d/\dot{\varepsilon}_c)$, occurs if one of the two viscosities drops before the other. This is possible if the activation energies contained in the diffusion terms of the two viscosities are sufficiently

different. The transient stage ends when the diffusion coefficients reach a relative stability and the variation of the viscosities becomes controlled by the geometrical terms.

1) We consider first the case in which η_s drops before η_{gb}. At the onset of the densification this case is described by the relations:

$$\eta_{gb} >> \eta_s \qquad \text{Eqn. 6.15}$$

However, as η_{gb} starts to drop too, the difference between the two viscosities reduces, and the term $\frac{\eta_{gb}}{\eta_{gb} + \eta_s}$ in Eqn. 6.12 decreases. Moreover, since this initial stage is characterized by a substantial predominance of the coarsening over the densification (associated to Eqn. 6.15), in this period the pores tend to grow, resulting in a decrease of $\frac{Kp}{\phi}$, namely of Σ. As a result $(\dot{\varepsilon}_d/\dot{\varepsilon}_c)$ can not be constant, but it is expected to decrease.

2) In the opposite case η_{gb} drops before η_s, so that:

$$\eta_{gb} << \eta_s \qquad \text{Eqn. 6.16}$$

At the onset of the densification $(\dot{\varepsilon}_d/\dot{\varepsilon}_c)$ is very low, due to the low value of η_{gb}, but it increases as η_s also drops and approaches η_{gb}. During this period densification is likely to prevail over coarsening and therefore Σ increases because of the reduced mean pore size, and further contributes to the increase of $(\dot{\varepsilon}_d/\dot{\varepsilon}_c)$.

6.1.3 Conclusions

In conclusion the development of the Swinkels and Ashby model leads to an expression for the ratio between densification rate and creep rate (Eqn. 6.12) that depends on the product of a kinetic term (the ratio of the viscosity for creep and densification) and the sintering stress.

If the surface redistribution process is negligible, such expression reduces to that introduced in section 2.2, where the kinetic term is constant and the ratio of the rates is proportional only to the sintering stress.

However, if the surface redistribution is a non negligible step for the densification, the kinetic term is typically not constant, as densification and creep are now governed by different kinetics. In this situation, unless the kinetics undergo temperature-related transient stages, the variations of the kinetic term tend to compensate the variations of the sintering stress, and the ratio between densification rate and creep rate is more likely to be constant.

If the kinetic mechanisms for coarsening and for densification are activated at different times during non-isothermal sintering, a transient stage takes place, during which the ratio of the rates is not expected to be constant. The variation of the kinetic term during the transient stage is associated to the imbalance between densification and coarsening, which also alters the sintering stress. For example: if, during the transient stage, densification prevails versus coarsening (due to its earlier activation), both the viscosity ratio and the sintering stress are expected to increase (and vice versa). As a result, in this situation the ratio between densification rate and creep rate is a good indicator of the evolution of the kinetics, and of the competition between densification and coarsening.

6.2 The powders' sintering behavior.

The sintering behavior of the various powders will be discussed here in relation to the considerations expressed in the previous sections of this chapter, and introducing theses regarding the effects of the dopants upon the sintering kinetics of the powders.

6.2.1 Al- and Bi-free powder: O.

The most interesting result provided by the sintering of **O** powders is the constancy of the ratio between densification rate and creep rate in the density range 55% - 95%. This result was expected on the basis of previous studies on ZnO compacts[7].

The result can be interpreted as the consequence of the equilibrium between densification and coarsening, which is indicated by the approximatively linear relation between the grain growth and the densification strain (in section 5.5 it we have: $\varepsilon_g = \kappa \varepsilon_d$, with $\kappa \sim 9$). Such an equilibrium can in fact be associated with a relative constancy of the sintering stress.

The constancy of the ratio between densification rate and creep rate is even more plausible if the surface redistribution plays a significant role in the sintering of this powder: in such a case, in fact, the ratio is determined by Eqn. 6.12, where if some variation occurs in the sintering stress, this tends to be balanced by a variation in the kinetic term.

[7]Having obtained this result with a procedure for the measurement of the creep strain different from that used in the other studies, confirms the validity of both techniques.

6.2.2 Al-doped powders: A and A2.

The sintering behavior of Al-doped, Bi-free powders is characterized by slower kinetics and variable ratio between densification rate and creep rate. These results can be explained in terms of defect chemistry.

The rates of diffusional transport in a crystal depend on the concentration of point defects. ZnO crystals exhibit n-type intrinsic conductivity as a consequence of oxygen deficiency, introduced either by interstitial zinc or oxygen vacancies. Considerations about the crystal structure of ZnO (wurtzite has large interstices that can readily accommodate excess zinc), zinc and oxygen diffusion coefficients and electrical conductivity led many authors to lend support to Frenkel rather than Schottky disorder [Kroger 1964, Hagemark and Chacka 1976 and Sukkar and Tuller 1982]. The ionization of ZnO can hence be expressed by the reaction:

$$ZnO \quad \Leftrightarrow \quad Zn_i^{\bullet\bullet} + \frac{1}{2} O_2(g) + 2e' \qquad \text{Eqn. 6.17}$$

which implies:

$$[Zn_i^{\bullet\bullet}] \, (P_{O_2})^{1/2} \, n^2 = K(T) \qquad \text{Eqn. 6.18}$$

Eqn. 6.18 relates the interstitial zinc ion concentration $[Zn_i^{\bullet\bullet}]$, which determines the rates of all sintering processes (see section 2.3.1), to the oxygen partial pressure P_{O_2} and the electron density n.

Now, according with Komatsu *et al* [1968], doping with aluminum leads to the substitution of Zn atoms with Al atoms, following the defect reaction:

$$Al_2O_3 \xrightarrow{ZnO} 2\,Al(Zn)^{\bullet} + 2\,ZnO + 2e' + 1/2\,O_2(g) \qquad \text{Eqn. 6.19}$$

It results that Al-doping produces an increase of the electron density and, from Eqn. 6.24, a depletion of the interstitial zinc concentration, which leads in turn to slower kinetics for densification, creep and coarsening during the first stage of the sintering.

The densification, however, appears less affected by this phenomenon (as in this stage the slope of ε_g vs. ε_d for Al-doped powders is lower than for **O** powders; see Fig.8). This can be explained assuming that the aluminum is preferentially distributed at the grain surface, so that the densification can still occur either by grain boundary diffusion (whose rate is though limited by the redistribution step) or by lattice diffusion, although at lower rate with respect to undoped powders.

As the temperature increases the value of K(T) in Eqn. 6.24 increases in such a way that the contribution of the reaction 6.25 to the electron density gradually becomes negligible. The surface diffusion is therefore gradually activated and the coarsening rate increases.

This situation corresponds to the last case discussed in section 6.1.3, as it is characterized by the initial prevalence of densification over coarsening, and by the recovery of coarsening as the surface diffusion becomes activated. Considering the densification by grain boundary diffusion (described by Eqn. 6.12), the model predicts in fact the low initial value of the ratio between densification rate and creep rate (due to the high value of η_s at the onset of the densification), and its subsequent increase (due to the increase of the sintering stress and the decrease of η_s)[7] .

The approximate constancy of the creep rate throughout the sintering of **A** and **A2**, shows that the increase of the diffusion coefficient for creep is balanced by the decrease of

[7] If lattice diffusion is the dominant mechanism, the increase of the ratio between densification and creep rate must be related to the increase of the sintering stress only.

the stress intensification factor ϕ as the densification proceeds, resulting in the constancy of the creep viscosity (see Eqn. 2.7). Since also the densification viscosity should hence be constant, in these powders the variations of the densification rate are caused only by variations of the sintering stress.

In the final stage ($T > 850^{O}C$, $\rho > 75\%$), considerable coarsening takes place in **A** with respect to **O** powders (Figs. 7 and 8), resulting presumably in an increase of the mean pore size and therefore in a decrease of the sintering stress, which leads to the drop of the ratio between densification and creep rate. This is explained considering that the smaller grain size of **A** is associated with higher driving force and smaller diffusional path for coarsening.

6.2.3 Liquid phase sintering: **B**, **AB** and **AB2**.

In the sintering of the bismuth-doped powders three different stages can be distinguished.

During the first stage, extending up to ~$725^{O}C$, no liquid phase is formed yet, and different sintering behaviors are observed in relation to the presence of aluminum.

In **AB** and **AB2** the low but increasing value of the ratio between densification rate and creep rate, associated with hindered coarsening, can be explained with the same argument used for **A** and **A2**.

The relatively high densification rate observed, to different extent, in each of the three powders, and the high coarsening rate of **B**, are related to a pre-eutectic effect of the bismuth, in this stage still distributed at the grain surface. In **B**, where no aluminum hinders the coarsening kinetics, this effect leads to a substantial predominance of the

coarsening versus the densification (Fig. 8), resulting in the decrease of the sintering stress and, consequently, of the ratio between densification rate and creep rate.

The second stage is a relatively brief period (extending from ~725^{o}C to ~750^{o}C for **B**, to ~760^{o}C for **AB2** and probably longer for **AB**, due to the retardant effect of Al on the liquid phase evolution) that however covers most of the densification range (from a relative density of 60% to 80-85% in **B** and **AB2**, from 53% until about 80% in **AB**), during which the intergranular liquid phase forms at the grain corners, giving rise to high densification rate and very high coarsening.

Although this stage begins before the eutectic temperature for the system Bi_2O_3-ZnO (740^{o}C), the high rates must be viewed as a consequence of the activation of a solution-precipitation process for the ZnO grains in contact with the liquid phase. At these temperatures, however, only a small fraction of the grain boundaries is wetted by the second phase [Gambino *et al*, 1989], which is mostly located at the grain boundary junctions, where it promotes coarsening. The densifying solution-precipitation process at the grain boundary is gradually activated as the contact angle between the grains and the liquid phase decreases. In this situation the densification is hence retarded with respect to coarsening, resulting in a decrease of the ratio between densification rate and creep rate, in agreement with the theoretical analysis in section 6.2.1 (when η_s drops before η_{gb}).

The relatively lower densification rate in **AB** promotes the decrease of the sintering stress, with the consequence that the ratio between densification rate and creep rate versus the density is more pronounced in **AB** than in **B** and **AB2**, where such ratio is actually almost constant (in **AB2** the excursion of the ratio ($\dot{\varepsilon}_d/\dot{\varepsilon}_c$) in the range of density 55%-85% is only about 1/6 of its value. Correspondingly, the plot of ε_g for **AB2** in fig.3 is hardy distinguishable from the one for **O**). This observation is explained by considering that the aluminum not only inhibits the kinetics of all powders, but also retards the

development of the liquid phase wetting, perhaps by reducing the solubility of the zinc in this phase. The lower degree of wetting of the grain boundaries by the liquid phase in **AB** is thus the probable cause of the reduced densification in this stage and, consequently, of the sharp drop of ($\dot{\varepsilon}_d/\dot{\varepsilon}_c$).

The final stage of the densification shows a steady decrease of the ratio between densification and creep rate. In **B** this corresponds presumably to a decrease of the sintering stress that is associated with the development of abnormal grain growth, grain coalescence, sequential filling of the smaller pores by the liquid phase and residual intragranular porosity. In **AB** and **AB2**, the decrease of the ratio is rather due to the stabilization of the creep rates at finite values, while the densification rates approach zero. This may be explained considering that at this stage the grain size of these powders (which approximately coincides with the creep diffusion path) is relatively small (at least if compared with that of **B**), while the diffusion coefficient is high and continues to increase as the contact angle between the grains and the liquid phase decreases with the temperature. The diffusion path for densification, instead, becomes greater than the grain size as several pores collapse already at relatively low density, due to the high inhomogeneity of the pore size distribution associated to liquid phase sintering [Park *et al*, 1984]. In conclusion, in this case the decrease of ($\dot{\varepsilon}_d/\dot{\varepsilon}_c$) express the faster growth of the viscosity for densification with respect to that for creep, not a variation of the sintering stress.

7 Conclusions

The constant heating rate sintering of six doped ZnO varistor precursor powders, differing one from the others by the concentration of Bi and Al, produced a wide spectrum of sintering behaviors.

Densification, creep and microstructure coarsening were found to be accelerated by the doping with Bi_2O_3, which gave rise during sintering to an intergranular liquid phase; while they were retarded in relation to the content of aluminum.

In powders not doped with aluminum or bismuth, the ratio between densification strain rate and creep strain rate was found to be constant in the density range 55% - 95%, while it was found to vary during the sintering if one or both dopants were added. By relating the trend of this ratio to the plot of the grain growth versus the temperature and densification strain, it was observed that a higher value of the slope of the grain growth relatively to non-doped powders corresponds to a decrease of the ratio between densification rate and creep rate, and vice versa.

An expression for the densification strain rate was derived within the frame of a model devised by Swinkels and Ashby [1980] where the densification is controlled by two processes in series, one of which (the redistribution of the matter along the pore surface) is governed by the same kinetic mechanism that presides over the coarsening process.

Following this theoretical approach, the constancy of the ratio between densification rate and creep rate appears more plausible, as the result of a balanced evolution of densification and coarsening, if the surface redistribution is a non-negligible step. On the other hand, if the kinetic mechanims for coarsening and densification are activated at different times during non-isothermal sintering, a transient stage takes place, during which

the ratio of the rates is expected to vary. In ZnO powders this appears to be the case when dopants such as aluminum or bismuth alter the temperature dependence of the kinetic mechanisms.

The sintering behavior of each powder was finally discussed in detail in terms of interaction between densification and coarsening, and introducing theses on the phenomenology of the dopants' effect.

Appendix

The densification rate equation for redistribution-controlled sintering.

The equation for $\dot{\varepsilon}_d$ in the case of redistribution-controlled sintering can be derived with a procedure analogous to that used by Chu [1990] for grain boundary limited sintering.

The procedure considers spherical particles of uniform size and packing distribution, connected by a neck. The geometry of the neck region is shown in Fig.17. Assuming that the surface redistribution occurs by surface diffusion[9], the component in the radial direction of the specific flux of atoms along the pore surface, as a function of the radial distance from the neck r, is:

$$F_s(r) = -\frac{Ds(T)}{\Omega\, kT}\left(\frac{\partial \mu}{\partial r}\right) \qquad \text{Eqn. A.1}$$

where Ds(T) is the coefficient of surface diffusion, Ω is the atomic volume, k is the Boltzman's constant, T is the absolute temperature and μ is the chemical potential.

The total flux of atoms at the distance r is then:

$$Js(r) = -\frac{2\,\pi\,(r+R)\,Ds}{\Omega\, kT}\left(\frac{\partial \mu}{\partial r}\right) \qquad \text{Eqn. A.2}$$

where R is the neck radius.

[9]The analysis does not differ substantially if the surface redistribution is governed by other mechanisms, such as evaporation-condensation, solution-precipitation, or lattice diffusion.

At the grain boundary-neck intersection the quasi steady-state condition implies (see Chu [1990]):

$$2Js(0) = Jgb(R) = \dot{\varepsilon}_d \frac{X^3}{\phi\ \Omega} \qquad \text{Eqn. A.3}$$

where Jgb is the flux through the grain boundary, and X is the center-to-center distance between the pores, approximatively coincident with the grain size.

Therefore, substituting Eqn.A.2 in Eqn.A.3:

$$\dot{\varepsilon}_d = -\frac{4\ \pi\ Ds}{kT} \frac{\phi\ R}{X^3} \left(\frac{\partial \mu}{\partial r}(0)\right) \qquad \text{Eqn. A.4}$$

The potential gradient can be expressed as:

$$\left(\frac{\partial \mu}{\partial r}\right) = -\Omega\ \gamma \left(\frac{\partial K}{\partial r}\right) = -\Omega\ \phi \left(\frac{\partial \Sigma}{\partial r}\right) \qquad \text{Eqn. A.5}$$

where K is the curvature of the neck surface.

If we can write the following approximation for the gradient at the neck-boundary intersection :

$$\left(\frac{\partial \mu}{\partial r}(0)\right) \sim \frac{\Delta \mu}{\Delta r} = -\Omega\ \gamma \frac{Kp\text{-}Kn}{\Delta r} = -\Omega\ \phi \frac{\Delta \Sigma s}{\Delta r} \qquad \text{Eqn. A.6}$$

where Δr is the diffusion distance along the radial direction, then the surface redistribution viscosity η_s can be written as follows:

$$\frac{1}{\eta_s} = \frac{4\ \pi\ Ds\ \Omega}{k\ T} \frac{\phi^2}{X^3} \frac{R}{\Delta r} \qquad \text{Eqn. A.7}$$

References

1. H.V. Atkinson, "Theories of Normal Grain Growth in Pure Single Phase Systems," *Acta Metall.*, **36** [3] 469-91 (1988).

2. L.K. Barrett and C.S. Yust, "Progressive shape changes of the Void During Sintering," *Trans. Metall. Soc.* AIME. 239 1172-80 (1967).

3. W. Beere, "Diffusional Flow and Hot Pressing: A Study on MgO," *J. Mat. Sci.*, **10** 1434-40 (1975).

4. D. Beruto, R. Botter and A.W. Searcy, "Influence of Temperature Gradient on Sintering: Experimental Tests of a Theory," *J. Am. Ceram. Soc.*, **72** [2] 232-35 (1989).

5. R.K. Bordia and G.W. Scherer,"On Constrained Sintering - III. Rigid Inclusions," *Acta Metall.*, **36** [9] 2411-16 (1988).

5. R.J. Brook, "Controlled Grain Growth," in *Treatise on Materials Science and Technology Vol. 9*, ed. F.F.Y. Wang (Academic Press, New York 1976) p. 331-65.

5. R.J. Brook, "Hot Pressing Dilatometry in the Study of Sintering Mechanisms," in *Sintering - Theory and Practice, Materials Science Monographs, Vol. 14*, ed. D. Kolar, S. Pejovnik, and M.M. Ristic (Elsevier Scientific Publishing Company, Amsterdam, 1982) p. 585-90.

7. J.E. Burke and J.H. Rosolowski, "Sintering," in *Treatise on Solid State Chemistry, Vol.4*, ed. N.B. Hannay (Plenum Press, New York 1976) p.621-59.

8. R.M. Cannon and W.C. Carter, "Interplay of Sintering Microstructures, Driving Forces, and Mass Transport Mechanisms," *J. Am. Ceram. Soc.*, **72** [8] 1550-55 (1989)

9. W.G. Carlson and T.K. Gupta, "Improved Varistor Nonlinearity Via Donor Impurity Doping," *J. Appl. Phys.*, **53** [8] 5746-53 (1982).

10. M.-Y. Chu, PhD Dissertation, (1990).

11. M.-Y. Chu, L.C. De Jonghe, and M.N. Rahaman,"Effect of Temperature on the Densification/Creep Viscosity During Sintering," *Acta Metall.*, **37** [5] 1415-20 (1989)

12. D.R. Clarke, "The Microstructural Location of the Intergranular Metal-Oxide Phase in a Zinc Oxide Varistor," *J. Appl. Phys.* **49** [4] 2407-11 (1978).

13. R.L. Coble, "Sintering Crystalline Solids. I. Intermediate and Final State Diffusion Models," *J. Appl. Phys.* **32** [5] 787-92 (1961).

14. R.L. Coble and R.M. Cannon, "Current Paradigms in Powder Processing," in *Materials Sciences Research Vol.11*, ed. H. Palmour III, R.F. Davis, T.M. Hare (Plenum Press, New York 1978) p.151-70.

15. R.T. DeHoff, "A Cell Model for Microstructural Evolution during Sintering," in *Materials Sciences Research, Vol. 16*, ed. G.C. Kuczynski, A.E. Miller and G.A. Sargent (Plenum Press, New York 1984) p. 23-24.

16. (a) L.C. De Jonghe and M.N. Rahaman, "Loading Dilatometer," *Rev. Sci. Instrum.* **55** [12] 2007-10 (1984).

17. (b) L.C. De Jonghe and M.N. Rahaman, "Pore Shrinkage and Sintering Stress," *Bull. Am. Cerm. Soc.*, **67** [10] c214-15 (1984).

18. L.C. De Jonghe and M.N. Rahaman, "Sintering Stress of Homogeneous and Heterogeneous Powder Compacts," *Acta Metall.*, **36** [1] 223-29 (1988)

19. L.C. De Jonghe and V. Srikanth, "Liquid-Phase Sintering of MgO-Bi_2O_3," *J. Am. Ceram. Soc.* **71** [7] c356-58 (1988).

20. L.C. De Jonghe, M.-Y. Chu and M.K.F. Lin, "Pore Size Distribution, Grain Growth, and the Sintering Stress," *J. Mat. Sci.* **24** 4403-08 (1989)

21. R.G. Dosch, B.A. Tuttle, and R.A. Brooks, "Chemical Preparation and Properties of High-Field Zinc Oxide Varistors," *J. Mater. Res.* **1** [1] 90-99 (1986).

22. S.K. Dutta and R.M. Spriggs, "Grain Growth in Fully Dense ZnO," *J. Am. Ceram. Soc.*, **53** [1] 61-62 (1970).

23. J. Frenkel, "Viscous Flow of Crystalline Bodies Under the Action of Surface Tension," *J. Phys. (USSR)*, **9** [5] 385-91 (1945).

24. J.P. Gambino, W.D. Kingery, G.E. Pike, L.M. Levinson, and H.R. Philipp, "Effect of the Heat Treatments on the Wetting Behavior of Bismuth-Rich Intergranular Phases in ZnO:Bi:Co Varistors," *J. Am. Ceram. Soc.*, **72** [4] 642-45 (1989).

25. T.J. Gardner and S.J. Lockwood, "Scale-Up of a Batch-Type Chemical Powder Preparation Process for High Field Varistor Fabrication," SANDIA Report 87-2194 (1988).

26. R.M. German, "Liquid Phase Sintering," (Plenum Press, New York 1985)

27. T.K. Gupta and R.L. Coble, "Sintering of ZnO: I, Densification and Grain Growth," *J. Am. Ceram. Soc.*, **51** [9] 521-25 (1968).

28. T.K. Gupta and R.L. Coble, "Sintering of ZnO: II, Density decrease and Pore Growth During the Final Stage of the Process," *J. Am. Ceram. Soc.*, **51** [9] 525-28 (1968).

29. K.I. Hagemark and L.C. Chacka, *J. Solid State Chem.*, **16**, 293 (1976).

30. M. Hillert, "On the Theory of Normal and Abnormal Grain Growth," *Acta Metall.*, **13** 227-38 (1965)

31. A. Jagota, P.R. Dawson and J.T.Jenkins, "An Anisotropic Continuum Model for the Sintering and Compaction of Powder Packings," *Mechanics of Materials* **7** (North Holland 1988) 255-69

32. D.L. Johnson, "Solid State Sintering Models," in *Materials Sciences Research, Vol. 13*, ed. G.C. Kuczynski (Plenum Press, New York 1979) p.97-106

33. J. Kim, T. Kimura, and T. Yamaguchi, "Effect of Bismuth Oxide Content on the Sintering of Zinc Oxide," *J. Am. Ceram. Soc.*, **72** [8] 1541-44 (1989).

34. K.M. Kimball and D.H. Doughty, "Aluminum Doping Studies on High Field ZnO Varistors," SANDIA Report 86-0713 (1987).

35. W. Komatsu, M.Miyamoto, S. Hujita, and Y Moriyoshi, "Effects of Dopants on Sintering of ZnO and NiO," *Yogyo Kyokaishi*, **76** [12] 407-12 (1968).

36. F.A. Kroger, "The Chemistry of Imperfect Crystals," (North Holland, Amsterdam 1964).

37. G.C. Kuczynski, "Towards the Understanding of the Process of Sintering," in *Sintering '85*, ed. G.C. Kuczynski, D.P. Uskokovic, H. Palmour III and M.M. Ristic (Plenum Press, New York 1985) p. 3-16

38. I.M. Lifshitz and V.V. Slevoz, *J. Phys. Chem. Solids*, U.S.S.R. **19** 315 (1961).

39. S.J. Lockwood and T.J. Gardner, "Washing and Filtration Study of the 1 Kg Batch-Type Chemical Powder Preparation Process for High Field Varistor Fabrication," SANDIA Report 87-2180 (1988).

40. P.Q. Mantas and J.L. Baptista, "Effect of Residual Moisture on the Sintering and Electrical Characteristics of ZnO Varistors," *Science of Ceramics*, **14** (1989) 985-89.

41. L.F. Norris and G. Parravano, "Sintering of ZnO," *J. Am. Ceram. Soc.*, **46** [9] 449-52 (1963).

42. H.-H. Park, S.-J Cho, and D.N. Yoon, "The Filling Process in Liquid Phase Sintering," *Metall. Trans.A*, **15A** (1984) p. 1075-80.

43. B.R. Patterson, v.d. Parkhe, and J.A. Griffin, "Effect of Particle Size Distribution on Sintering," in *Sintering '85*, ed. G.C. Kuczynski, D.P. Uskokovic, H. Palmour III and M.M. Ristic (Plenum Press, New York 1985) p. 43-52.

44. M.N. Rahaman and L.C. De Jonghe, "Creep-Sintering of ZnO," *J. Mat. Science*, **22** (1987) 4326-30.

45. M.N. Rahaman, L.C. De Jonghe, and M.-Y. Chu, "Densification and Shear Deformation in $YBa_2Cu_3O_{6+}\delta$ Powder Compacts," *Advanced Ceramic Materials*, **3** [4] 393-97 (1988).

46. F.N. Rhines and R.T. DeHoff, "Channel Network Decay in Sintering," in *Materials Sciences Research, Vol. 16*, ed. G.C. Kuczynski, A.E. Miller and G.A. Sargent (Plenum Press, New York 1984) p. 49-61.

47. G.M. Safronov, V.N. Batog, T.V. Stepanyuk, and P.M. Fedorov, "Equilibrium Diagram of the Bismuth Oxide - Zinc Oxide System," *Russ. J. Inorg. Chem.* (Engl. Transl.), **16** [3] 460-61 (1971).

48. A.W. Searcy, "Driving Force for Sintering of Particles with Anisotropic Surface Energies," *J. Am. Ceram. Soc.*, **68** [10] c267-68 (1985).

49. A.W. Searcy, "Theory for Sintering in Temperature Gradients: Role of long-Range Mass Transport," *J. Am. Ceram. Soc.*, **70** [3] c61-62 (1987).

50. T. Senda and R.C. Bradt, "Grain Growth in Sintered ZnO and ZnO-Bi_2O_3 *J. Am. Ceram. Soc.*, **73** [1] 106-14 (1990).

51. M.H. Sukkar and H.L. Tuller, in "*Advances in Ceramics vol.7* " (American Ceramic Society, Ohio, 1982), p.71.

52. F.B. Swinkels and M.F. Ashby, "Role of Surface Redistribution in Sintering by Grain Boundary Transport", *Powder Metallurgy*, 1 p.1 (1980).

53. T. Takemura and M. Kobayashi, "Effects of Aluminum as Dopant on the Characteristics of ZnO Varistors,"

54. C. Wagner, "Theorie der Alterung von Niederschlagen durch Umlosen (Ostwald-Reifung)", *Zeitschrift fur Elektrochemie* **65** [7/8] 581-91 (1961)

55. O.J. Whittemore and S.L. Powell, "Effects of Oxygen Pressure and Water Vapor on Sintering of ZnO," in *Materials Sciences Research, Vol. 16*, ed. G.C. Kuczynski, A.E. Miller and G.A. Sargent (Plenum Press, New York 1984) p. 137-44.

56. O.J. Whittemore and J.A. Varela, "Pore Distribution and Pore Growth During the Initial Stages of Sintering," in *Materials Sciences Research, Vol. 13*, ed. G.C. Kuczynski (Plenum Press, New York 1979) p.51-60.

57. O.J. Whittemore and J.A. Varela, "Initial Sintering in ZnO" *J. Am. Ceram. Soc.*, **64** [11] c154-55 (1981).

58. J.M. Vieira and R.J. Brook,"Kinetics of Hot-Pressing: the Semilogaritmic Law," *J. Am. Ceram. Soc.*, **67** [4] 245-49 (1984).

59. J. Wong, "Sintering and Varistor Characteristics of ZnO-Bi_2O_3 ceramics," *J. Appl. Phys.* **51** [8] 4453-59 (1980).

The six powders

O : ZnO 99.5 mol% , CoO 0.25 mol% , MnO 0.25 mol%

A : same as **O** + Al 340 ppm

A2 : same as **O** + Al 142 ppm

B : ZnO 98.94 mol% , CoO 0.25 mol% , MnO 0.25 mol% , Bi_2O_3 0.56 mol%

AB : same as **B** + Al 340 ppm

AB2: same as **B** + Al 142 ppm

Sintering Data Table 1

Powders:		O	A	A2	B	AB	AB2
Non-loaded samples	ρ_o (%)	48.9	49.5	49.6	48.0	47.65	48.6
	ρ_f (%)	99.0	99.1*	98.7	97.1	98.4	98.7
	ϵ_ρ	0.235	0.231*	0.229	0.235	0.242	0.230
	ϵ_z	0.235	0.233*	0.237	0.253	0.259	0.256
Loaded samples	load (MPa)	0.25	0.25	0.25	0.20	0.20	0.20
	ρ_o (%)	48.7	49.4	49.5	48.2	47.5	48.4
	ρ_f (%)	99.1	99.3*	99.5	97.8	99.5	99.5
	ϵ_ρ	0.236	0.233*	0.230	0.236	0.246	0.240
	ϵ_c	0.037	0.033*	0.034	0.126	0.175	0.156

All the measurements are taken at Temp.= 1,000°C, except those marked with (*), which are taken at Temp.= 1,050°C

ρ_o = initial density, % of the theoretical value of 5.61 g/cm^3 for O, A and A2; of 5.67 g/cm^3 for B, AB and AB2

ρ_f = final density

ϵ_ρ = final densification strain

ϵ_c = final creep strain

mean grain size

Temp. C	O	A	A2	B	AB	AB2
green	55	80	70	60	60	60
710				180	68	92
730	99	87	97	300	80	
750-760		93	105		130	290
790-800	160	115	120	1270	235	390
850		150				
900	470	695			650	
1000*	1950		1100	7000	1100	1150
1040*		800		24000	1900	
1100*					4100	

The mean grain sizes are expressed in nm. All samples were rapidly quenched from the reported temperatures, except those sintered to the temperatures marked with (*), which were cooled slowly to ambient temperature.

Table 2

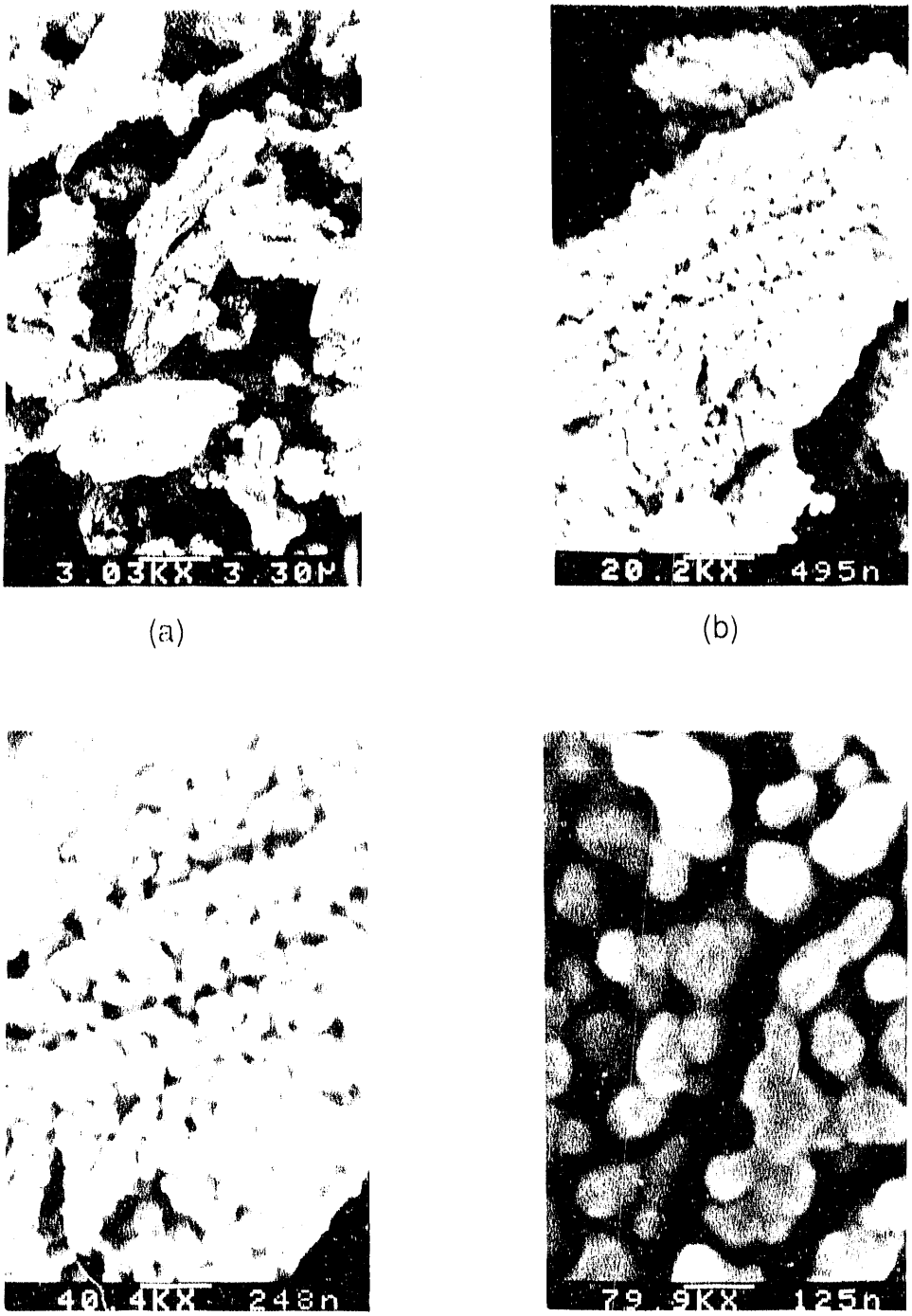

Fig. 1 - SEM micrographs of green powders

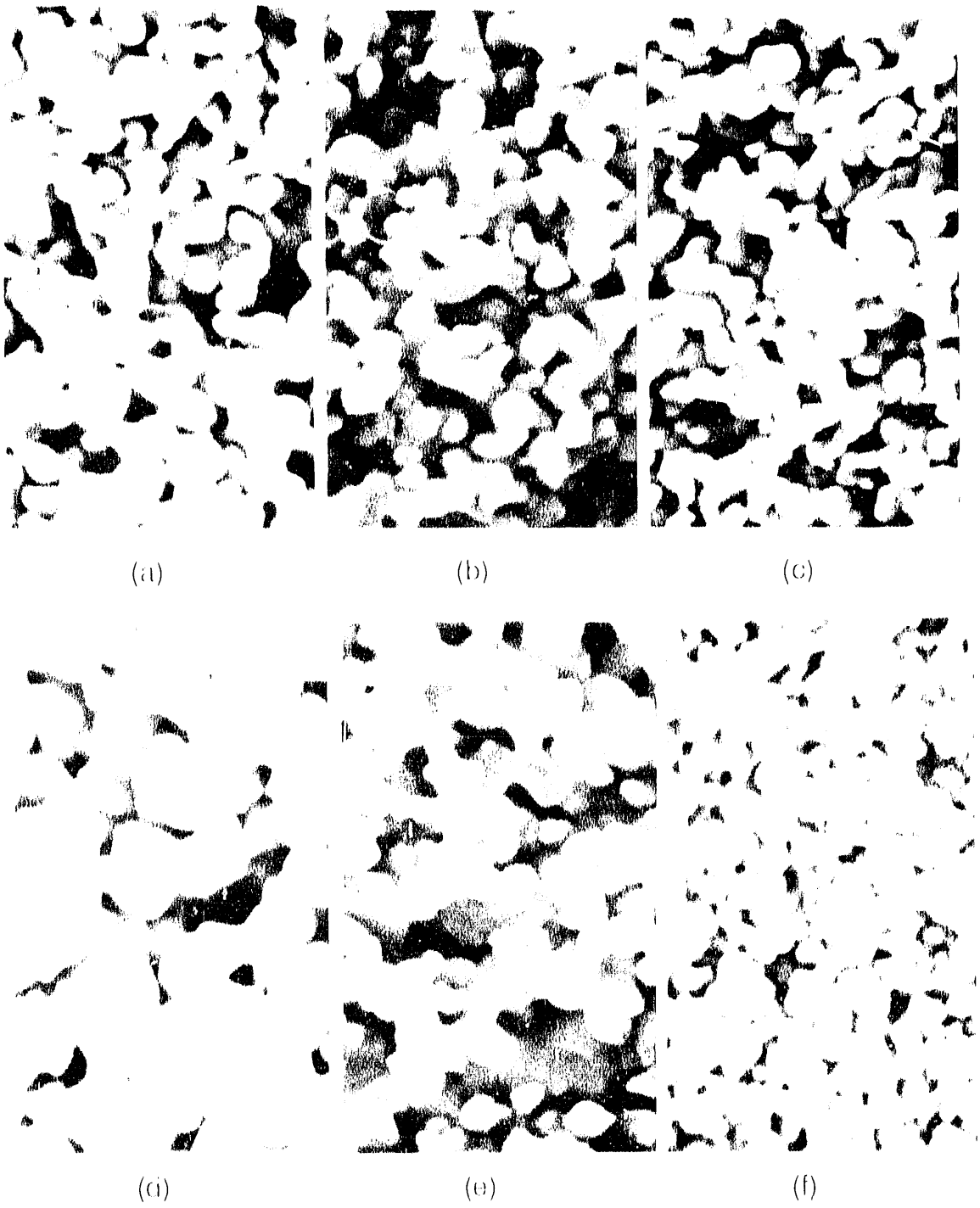

Fig. 2 - SEM fracture surfaces

(a) **O**: ε_d = .044, T = 730°C; (b) **A2**: ε_d = .042, T = 730°C; (c) **A**: ε_d = .050, T = 750°C
(d) **B**: ε_d = .048, T = 710°C; (e) **AB2**: ε_d = .047, T = 710°C; (f) **AB**: ε_d = .040, T = 730°C

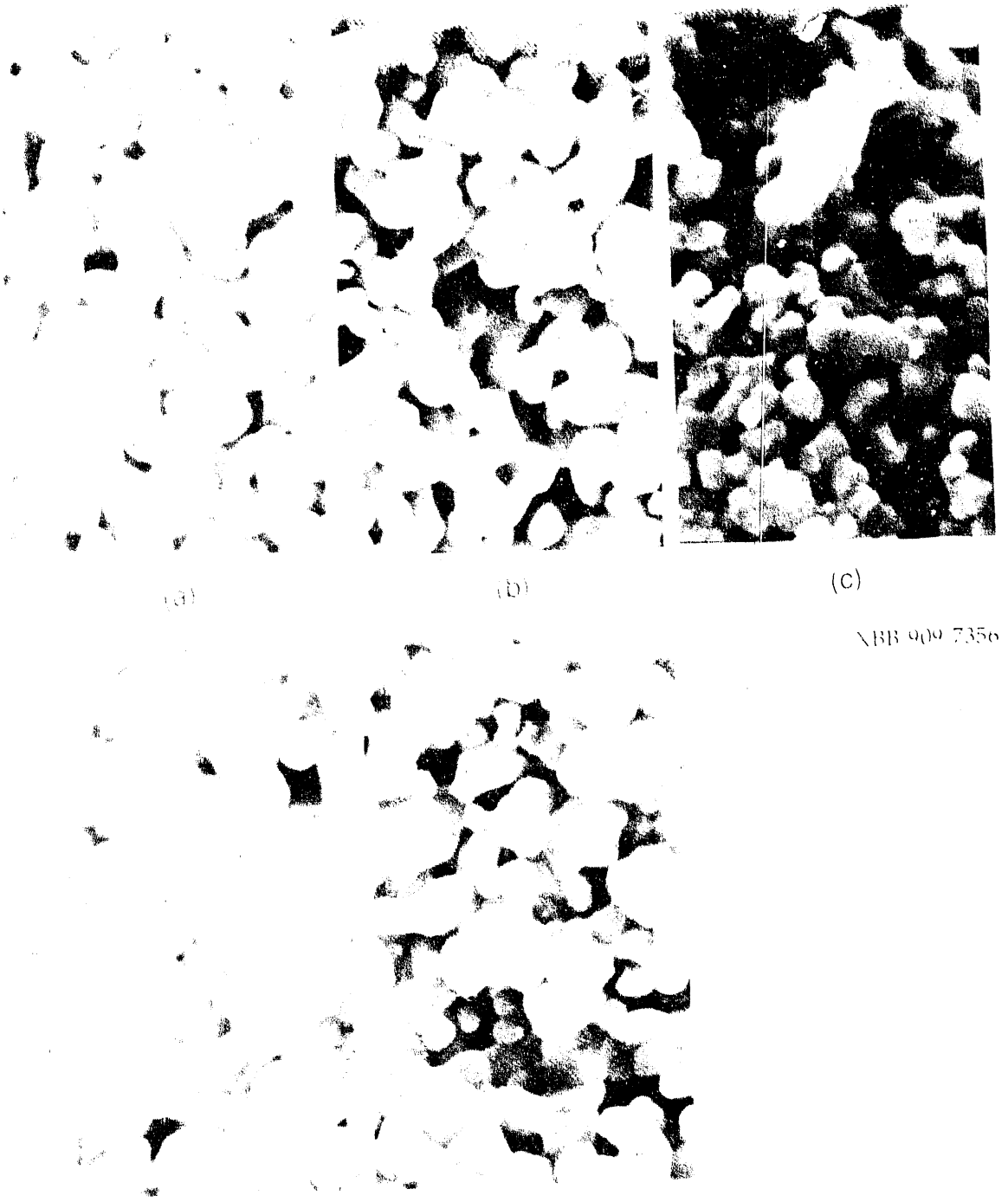

XBB 909-7356

Fig. 3 - SEM fracture surfaces

(a) O (β = 0.15, T = 500°C), (b) A2 (β = 0.90, T = 500°C), (c) A (β = 1.087, T = 800°C)
(d) B (β = 1.20, T = 750°C), (e) AB (β = 1.25, T = 800°C)

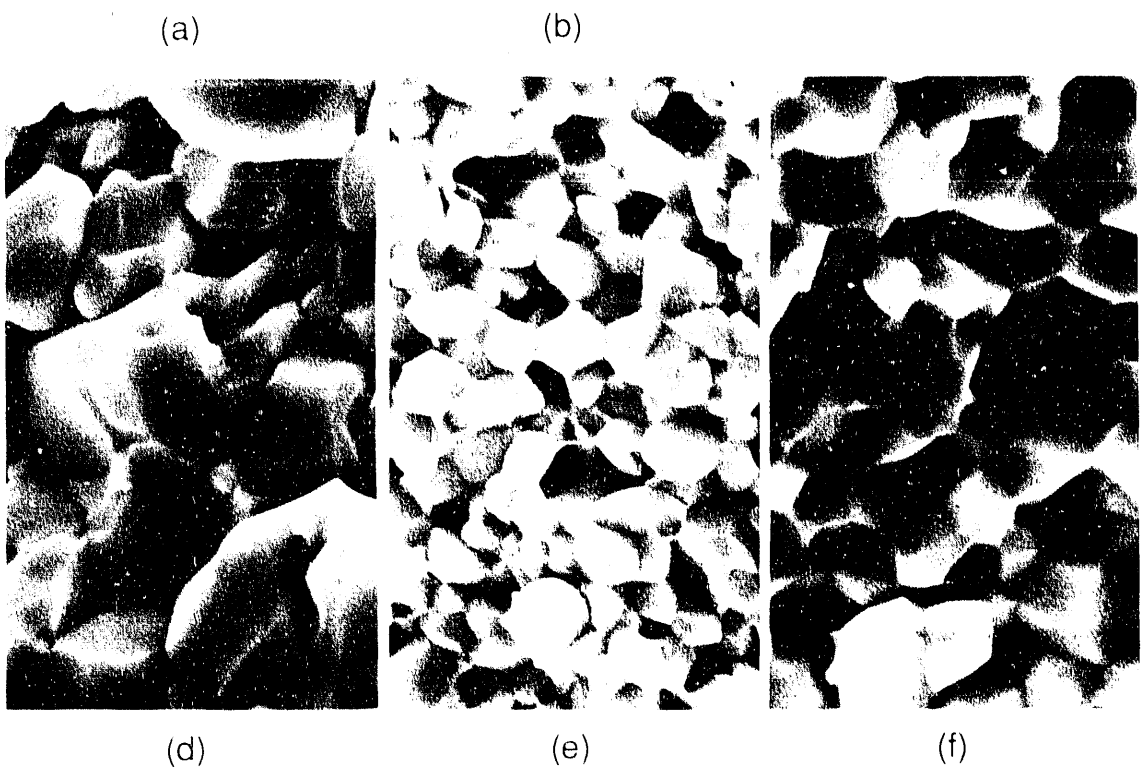

Fig. 4 - SEM polished and fracture surfaces

(a) **O**: ε_d= .215, T= 886°C, polished; (b) **A**: ε_d= .175, T= 900°C, polished
(d) **B**: ε_d= .216, T= 790°C; (e) **AB2**: ε_d= .215, T=800°C; (f) **AB**: ε_d= .240, T= 900°C

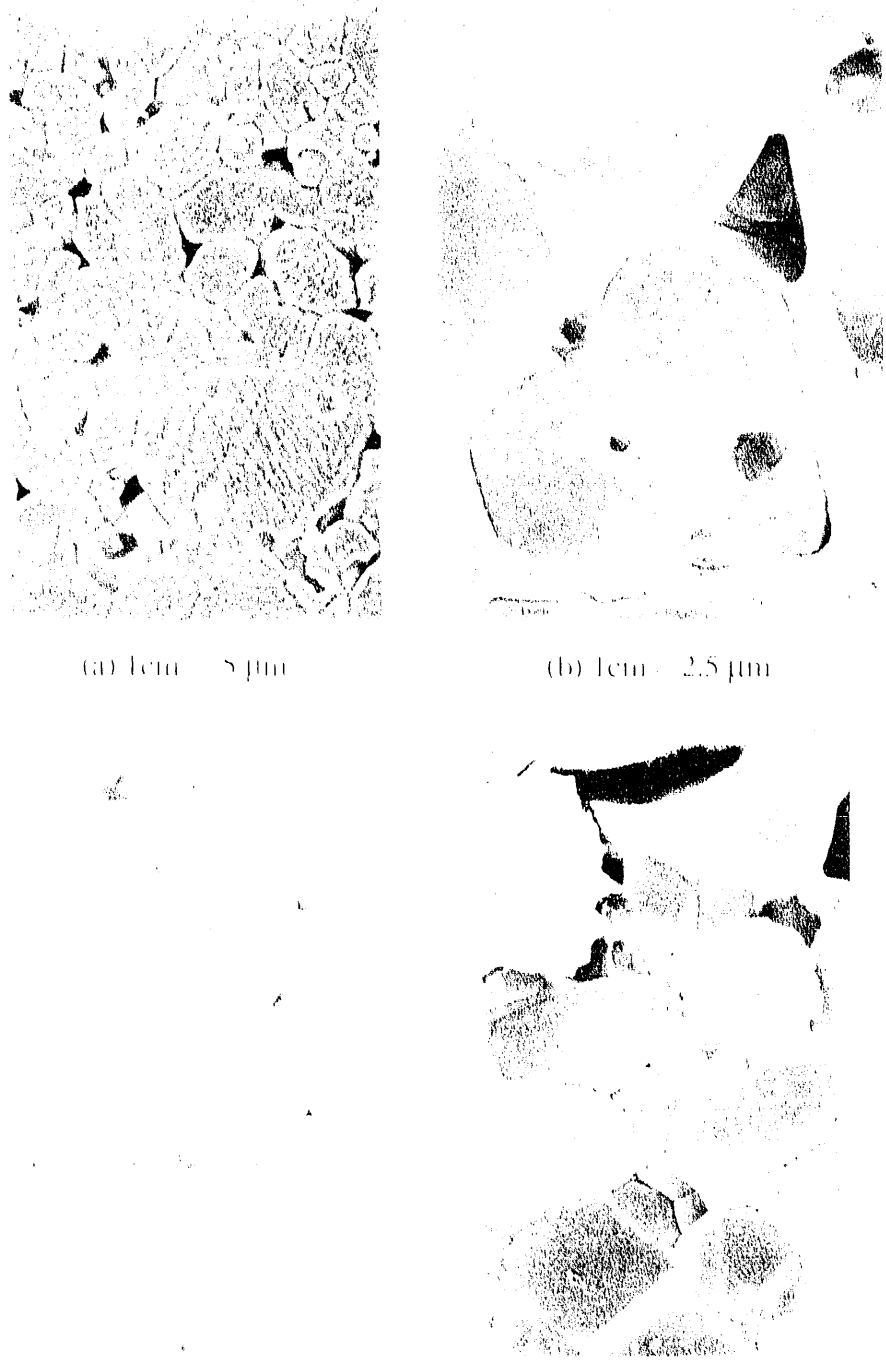

Fig. 5 - SEM micrographs of fully sintered compacts.

(a) B: 990°C, polished and thermally etched; (b) B: 1040°C
(c) AB: 1040°C, polished and thermally etched; (d) AB: 1100°C

Fig. 6 - mean grain size vs. temperature

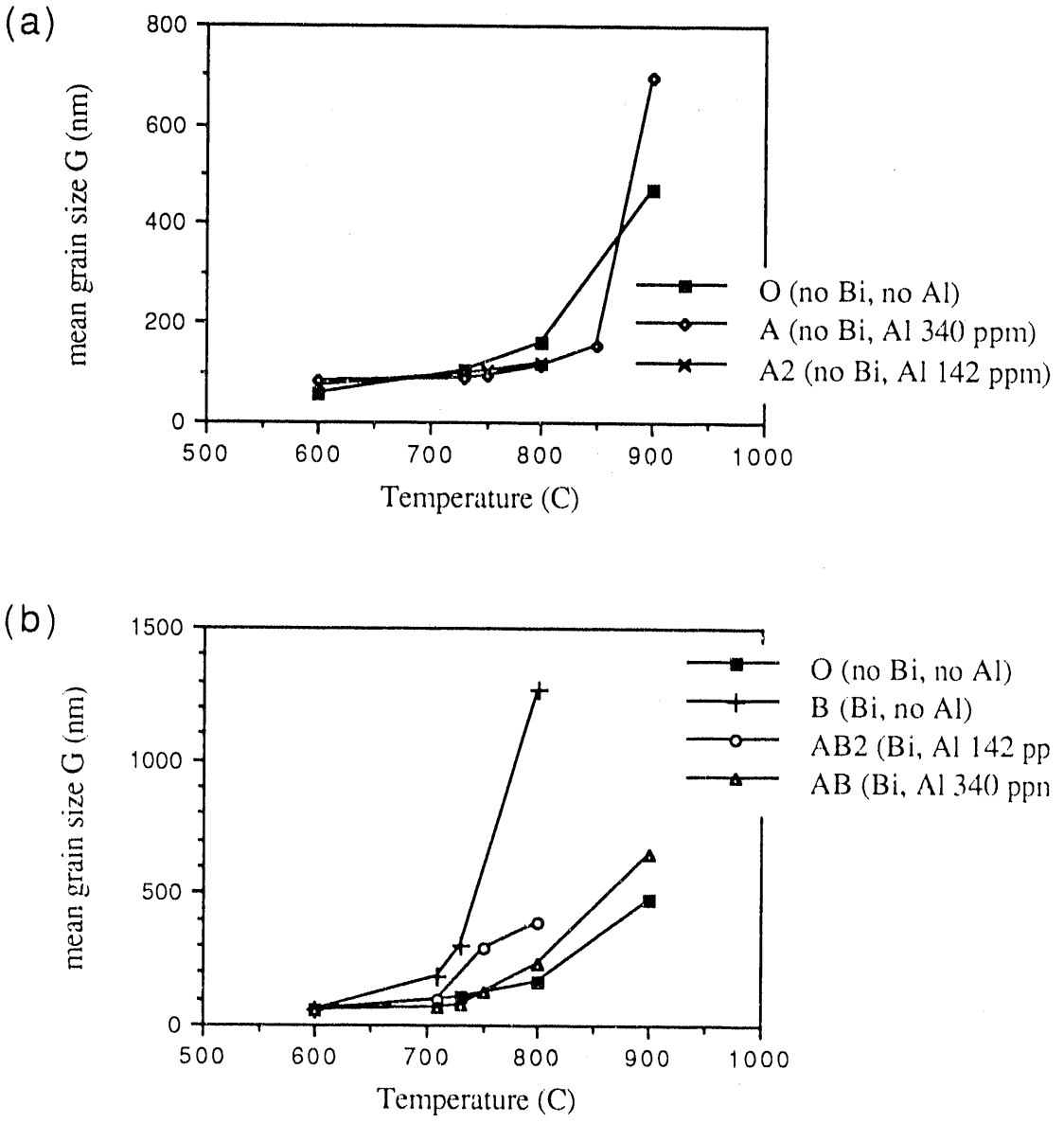

Fig. 7 - grain growth vs. temperature

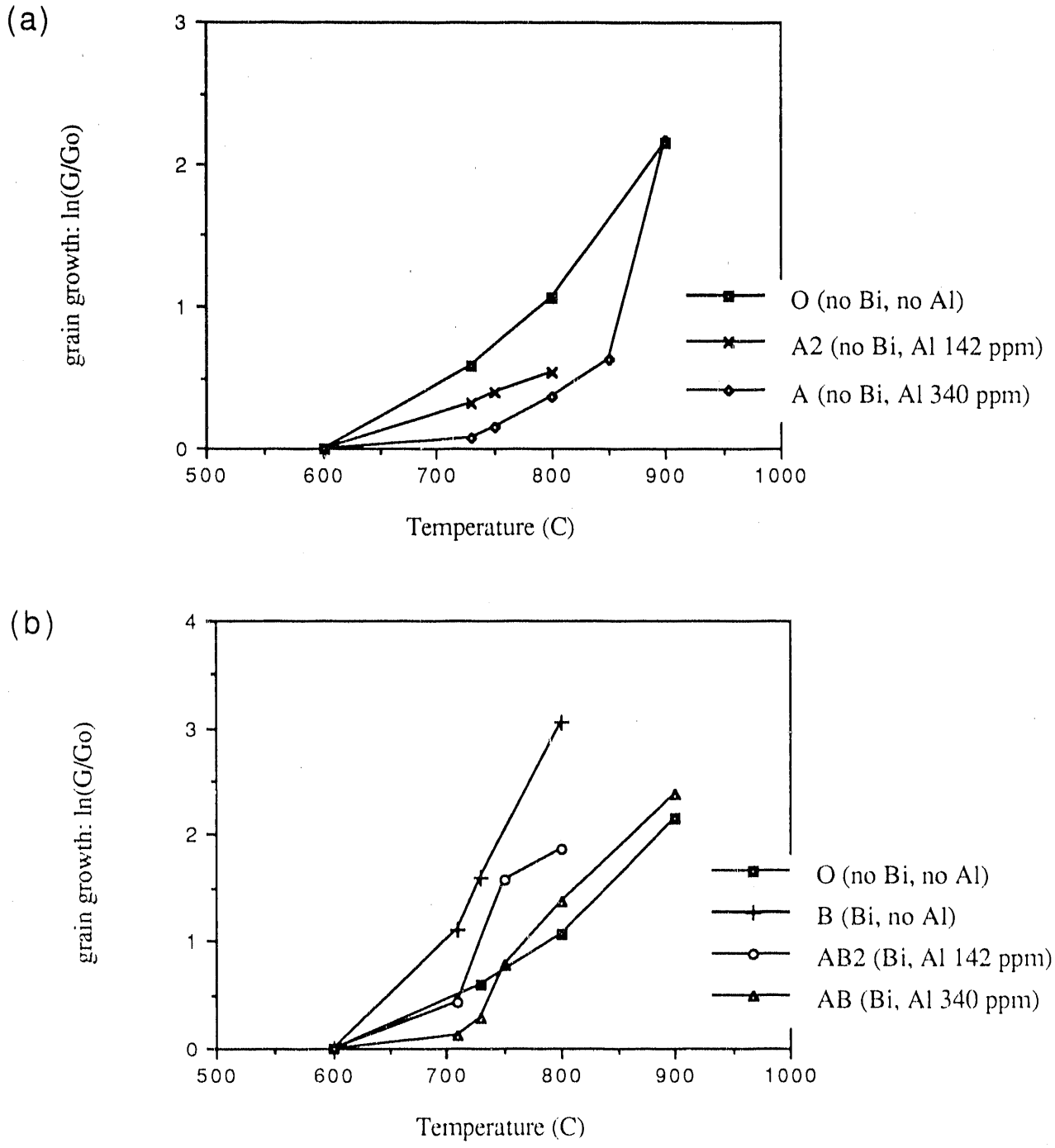

Fig. 8 - grain growth vs. densification

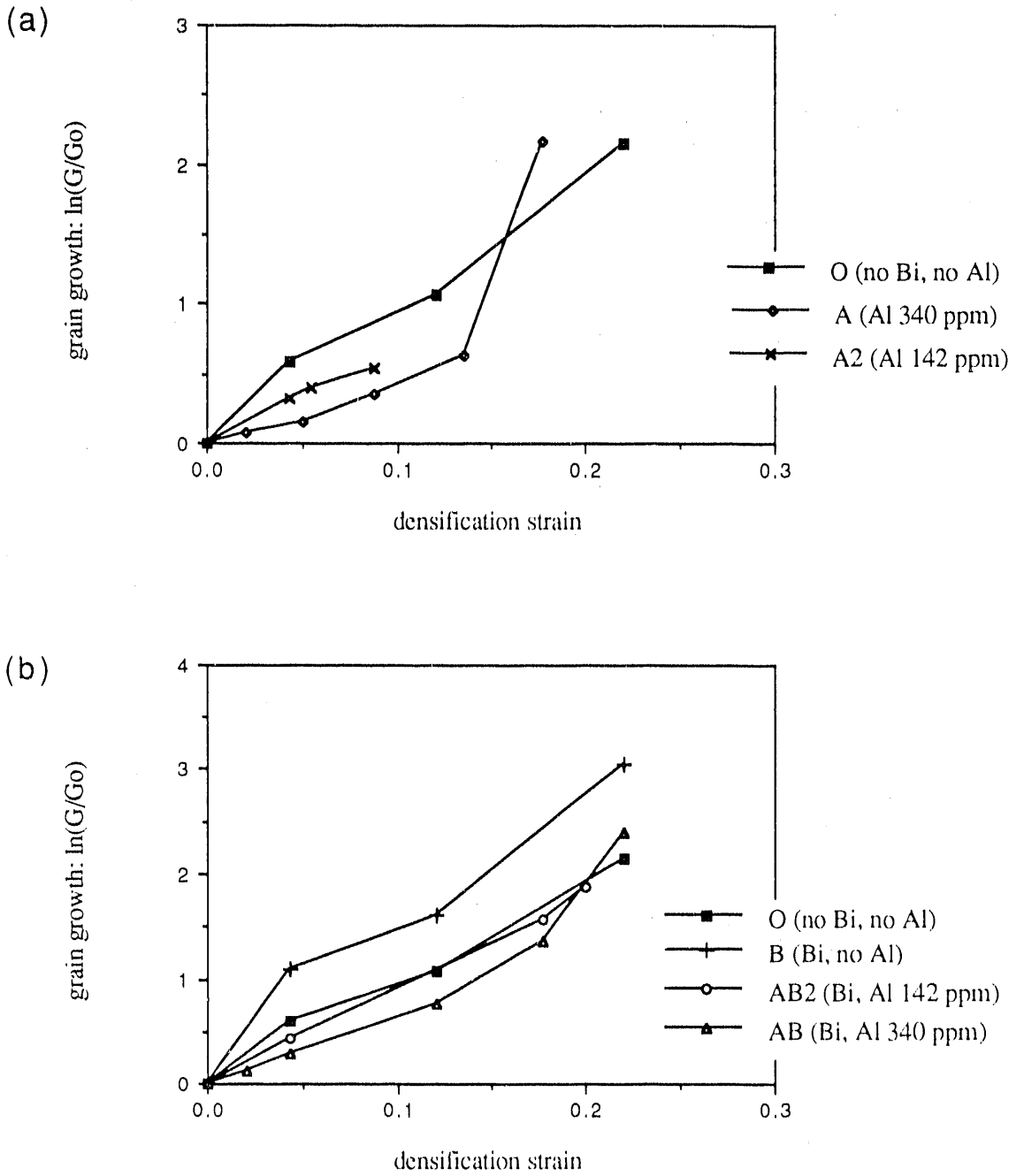

Fig. 9 RELATIVE DENSITY

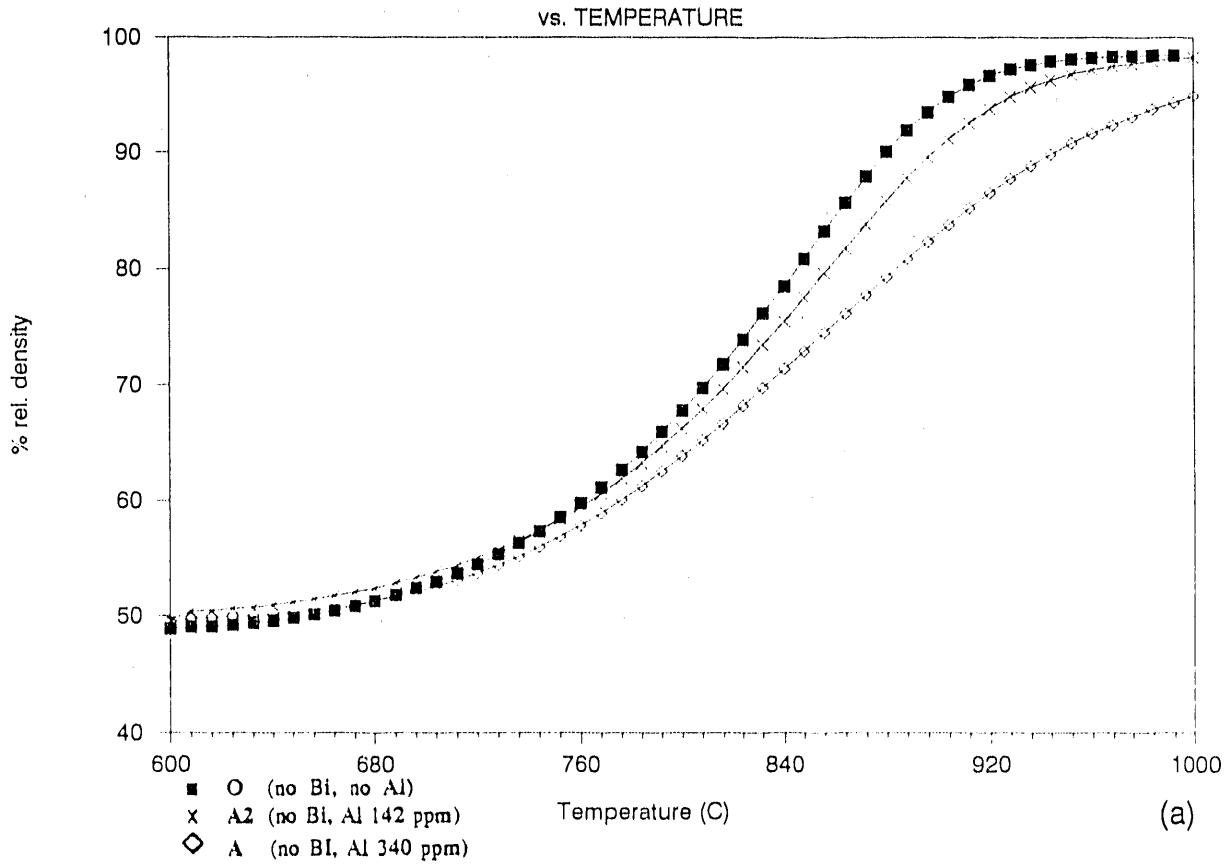

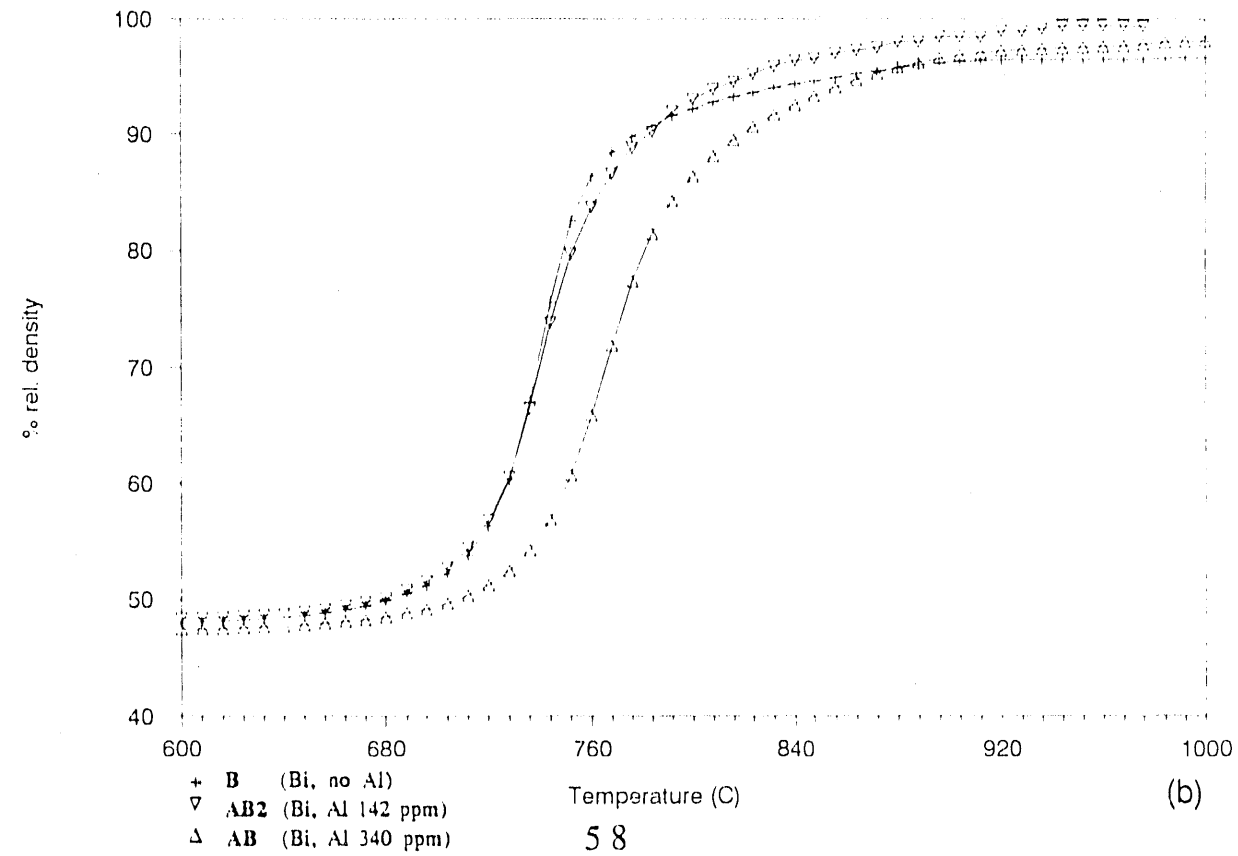

Fig. 10 CREEP STRAIN
vs. TEMPERATURE

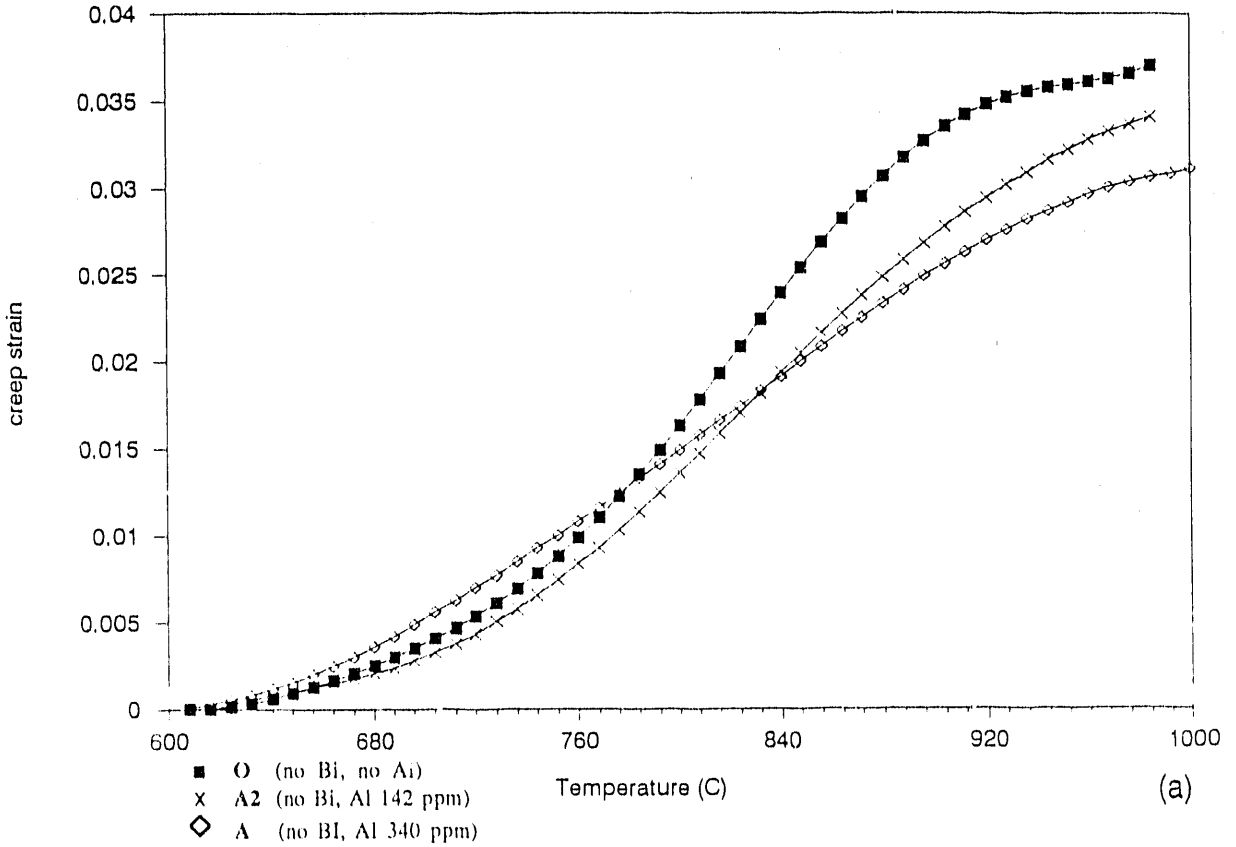

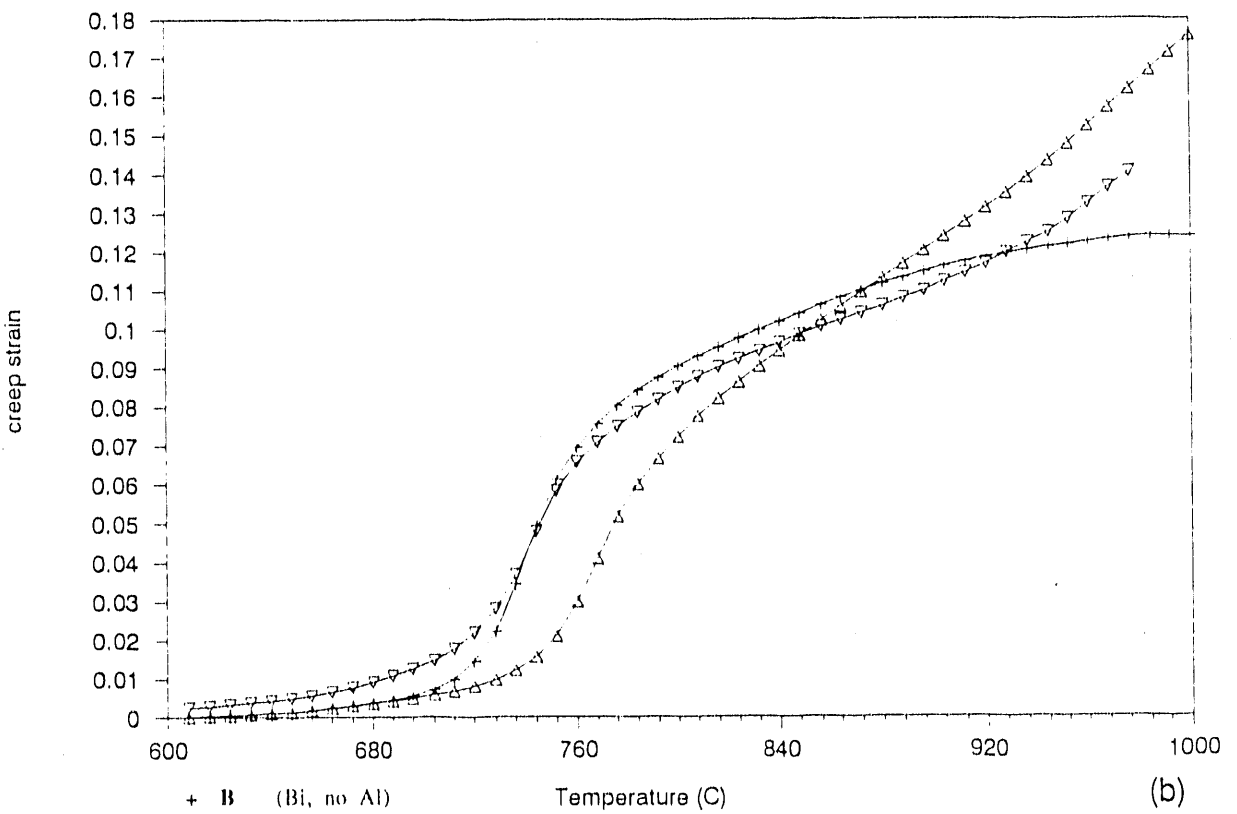

Fig. 11 **DENSIFICATION STRAIN RATE**
vs. TEMPERATURE

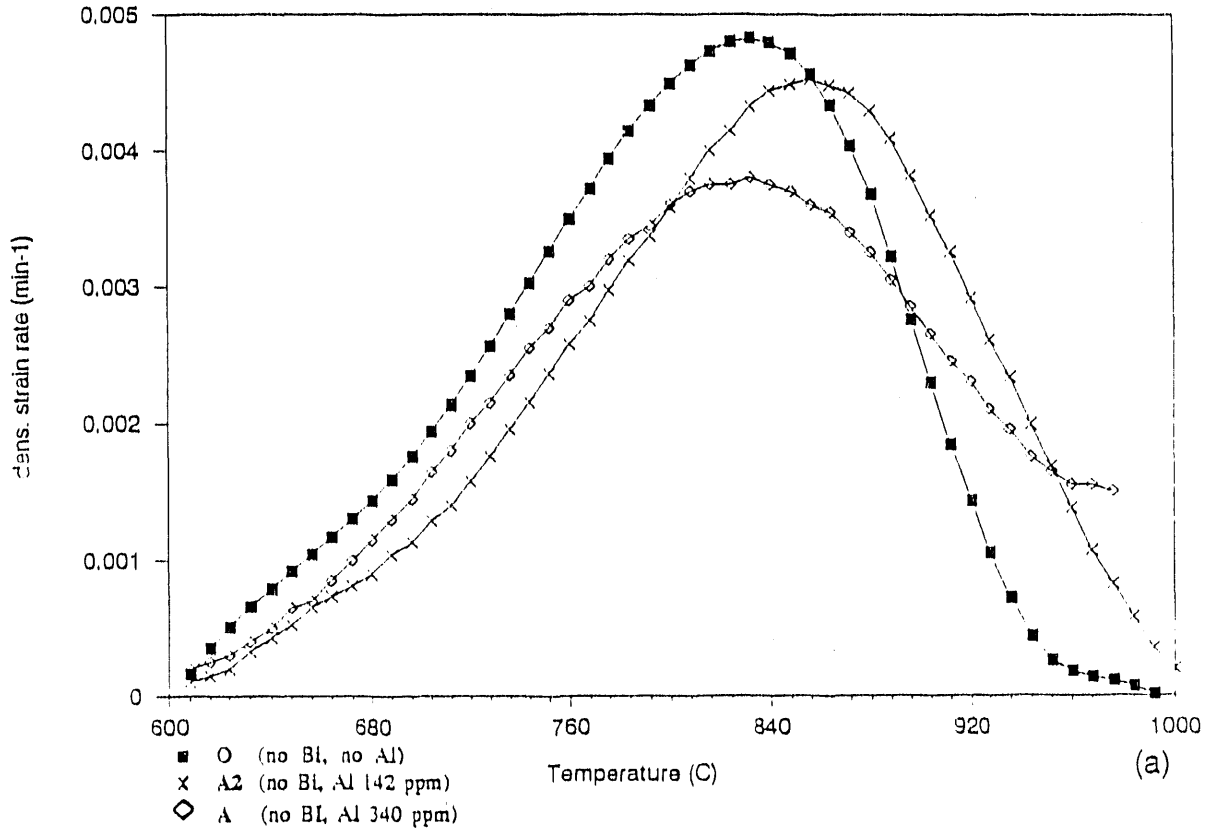

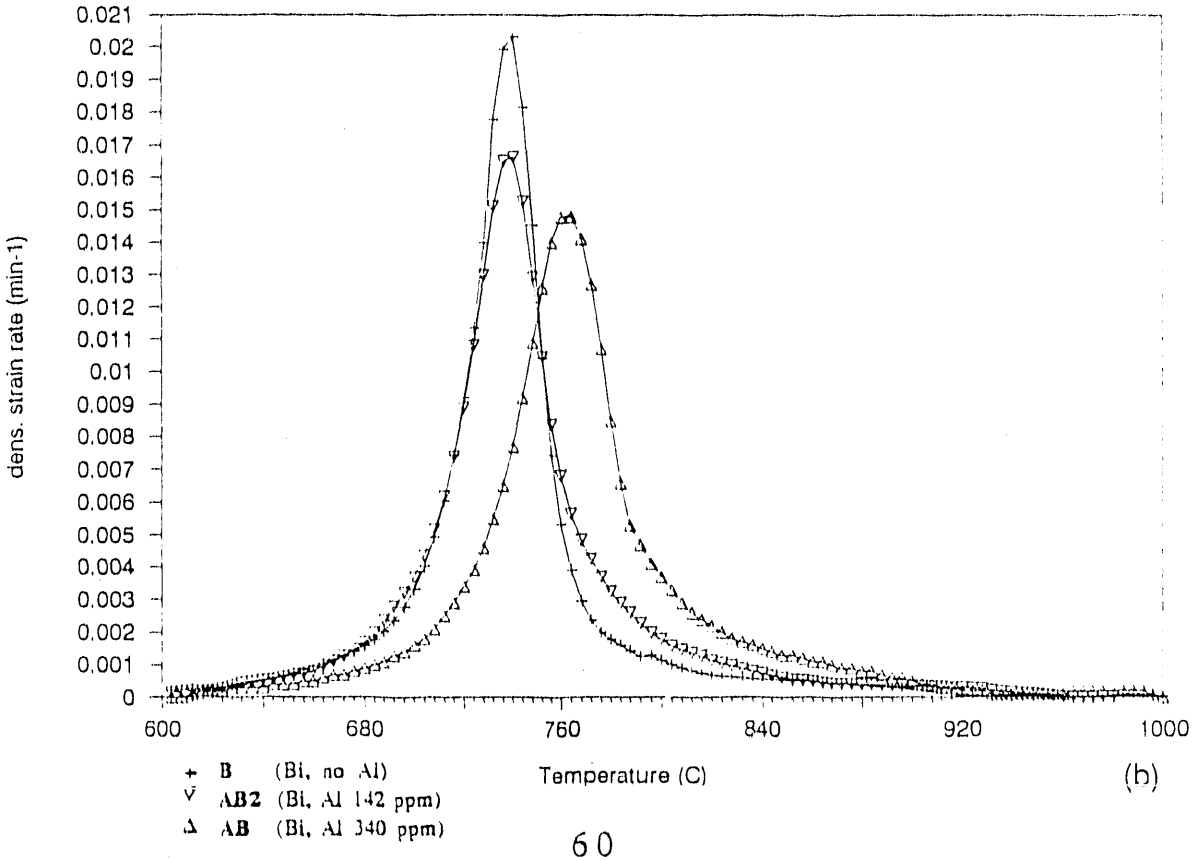

Fig. 12 **CREEP STRAIN RATE**
vs. TEMPERATURE

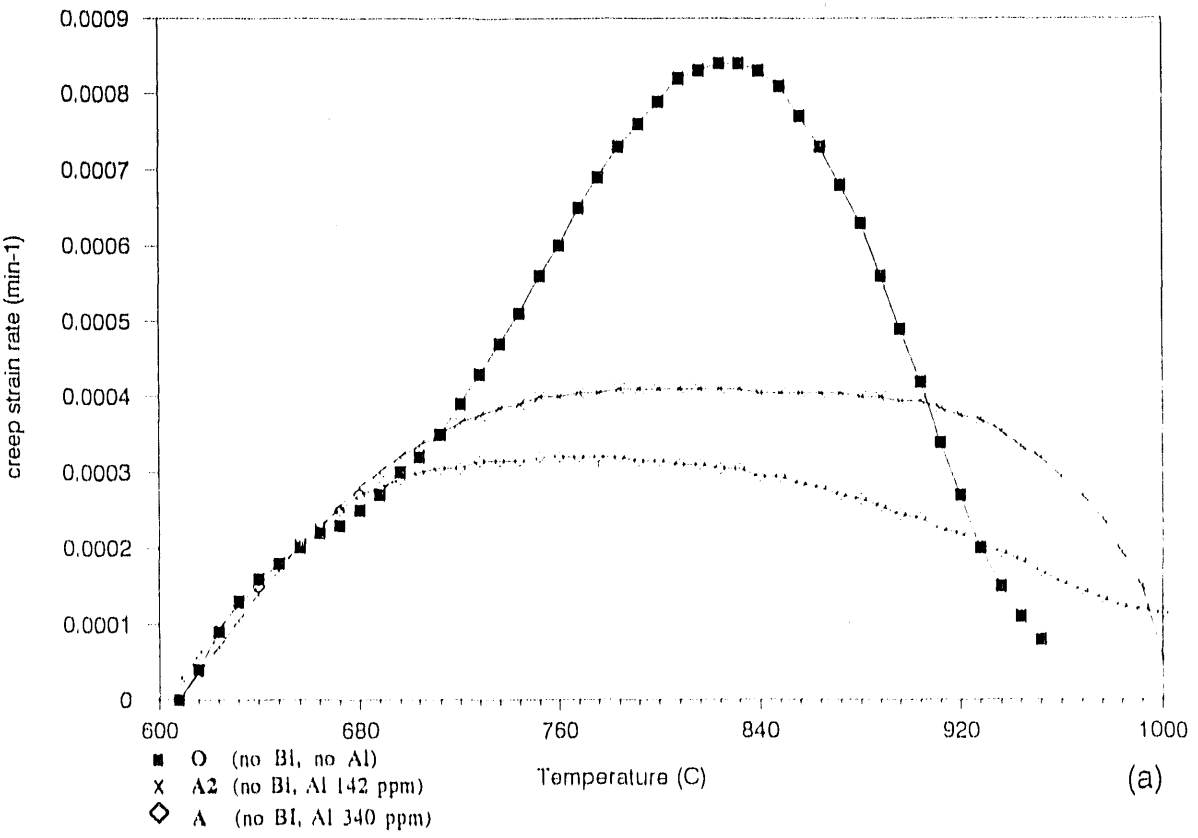

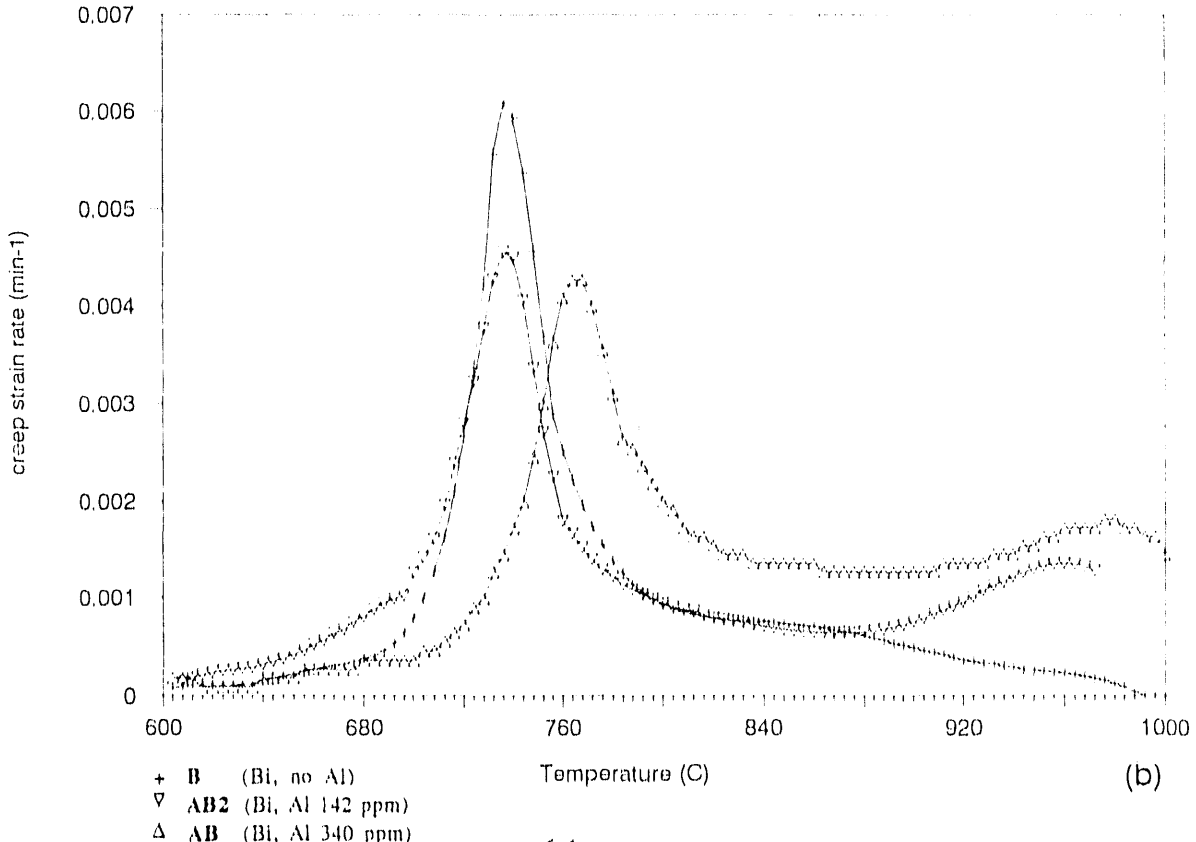

Fig. 13 RATIO BETWEEN DENS. RATE AND CREEP RATE vs. TEMPERATURE

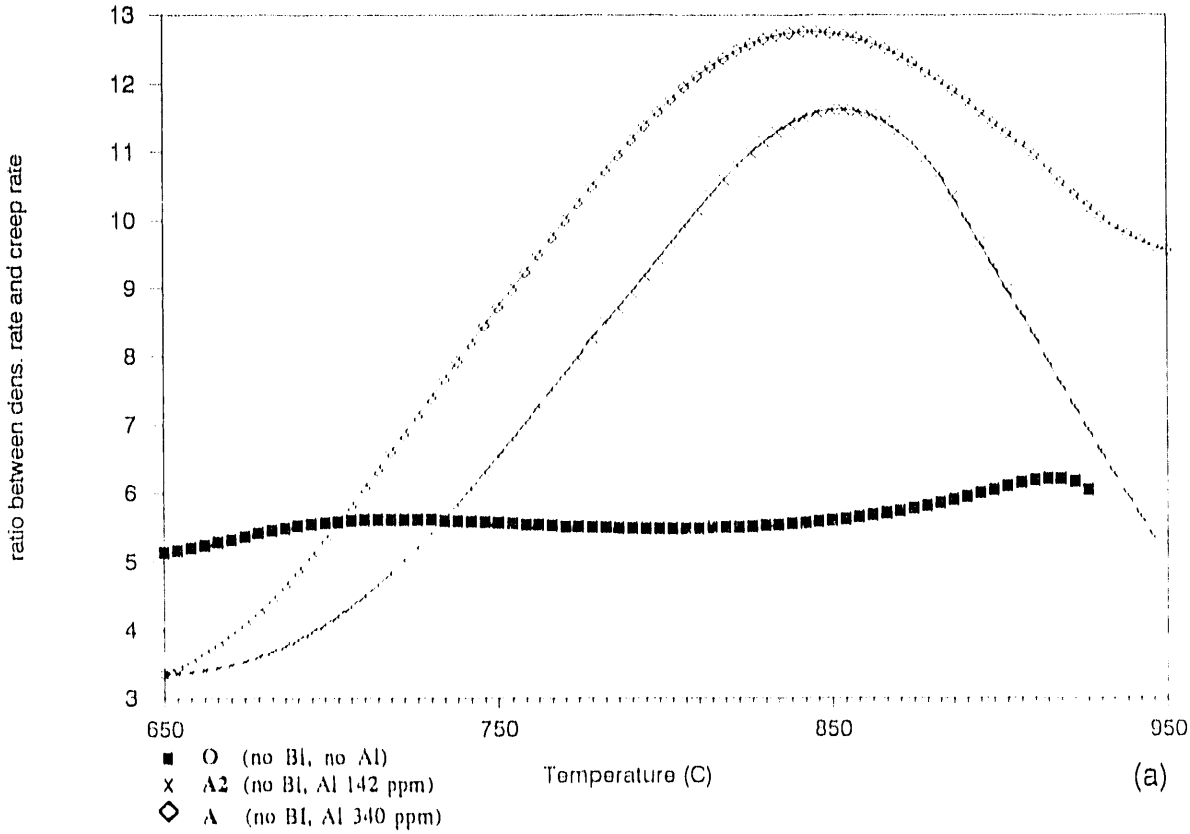

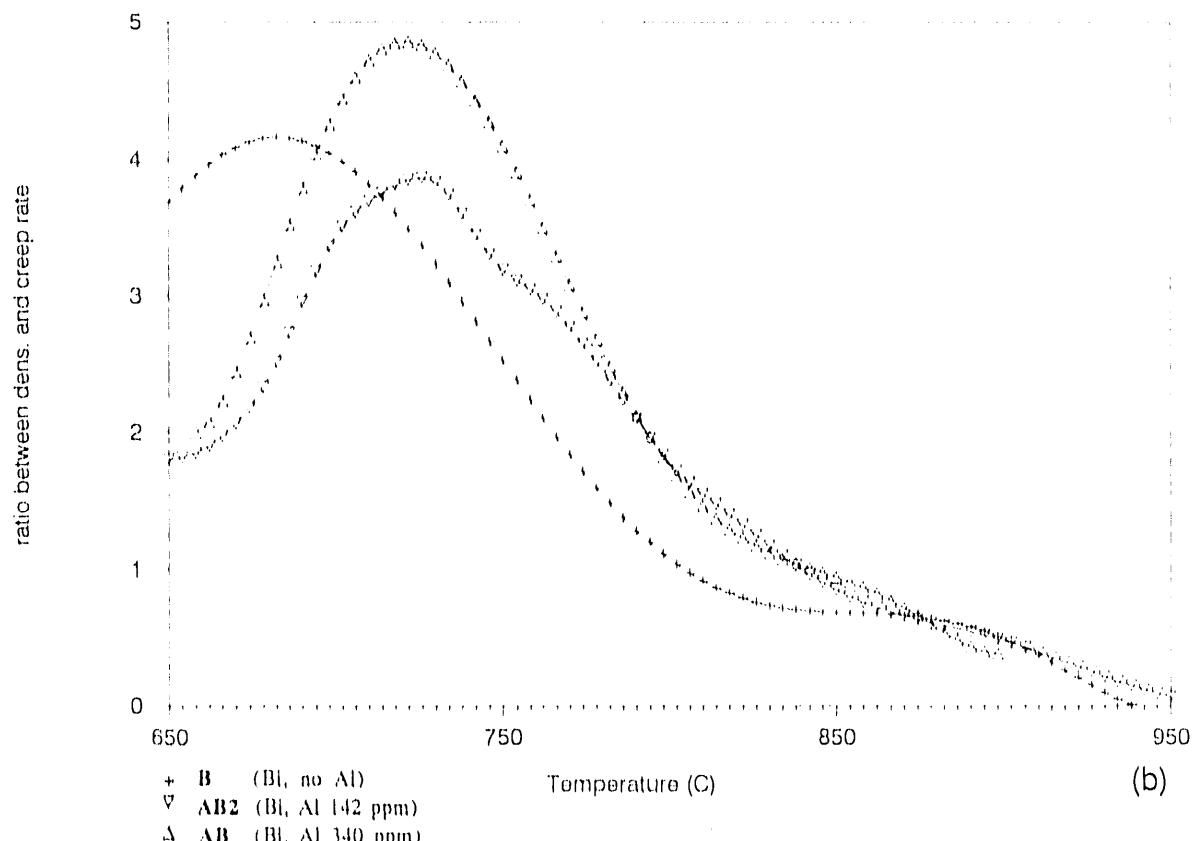

Fig. 14 CREEP STRAIN RATE vs. DENSITY

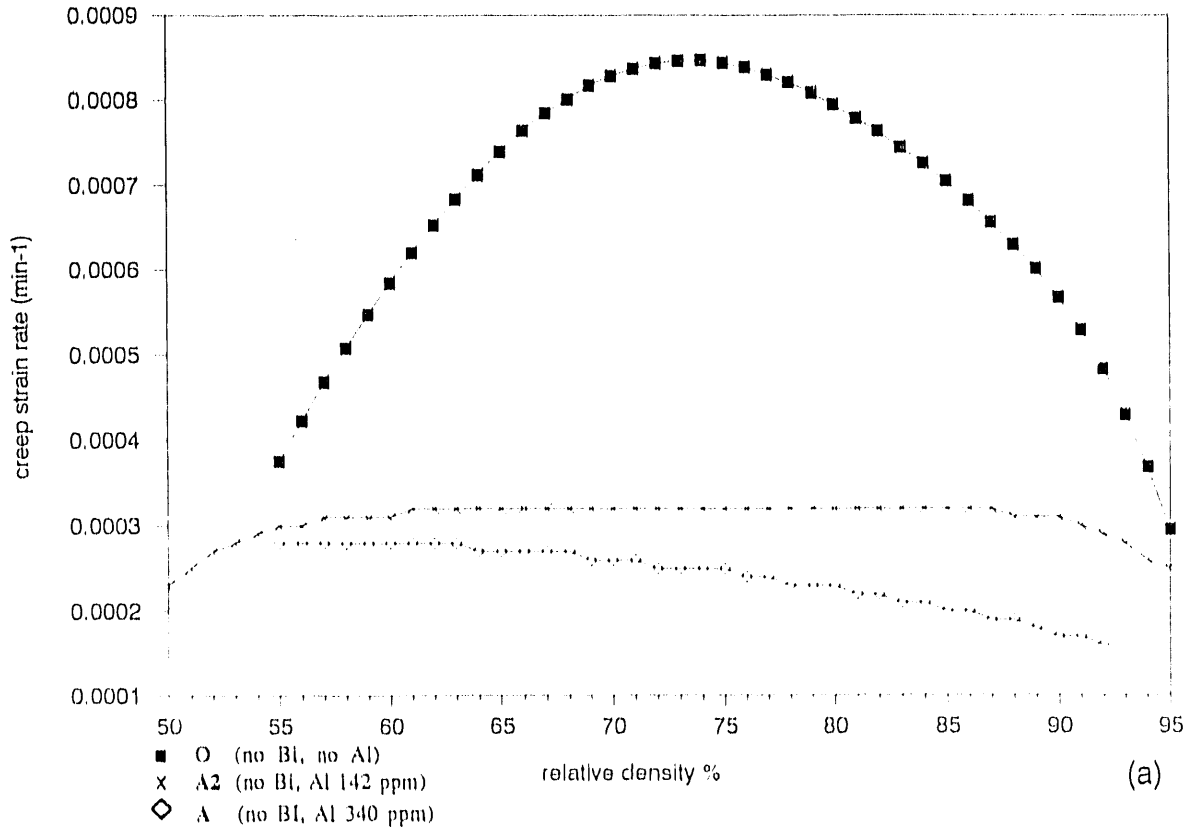

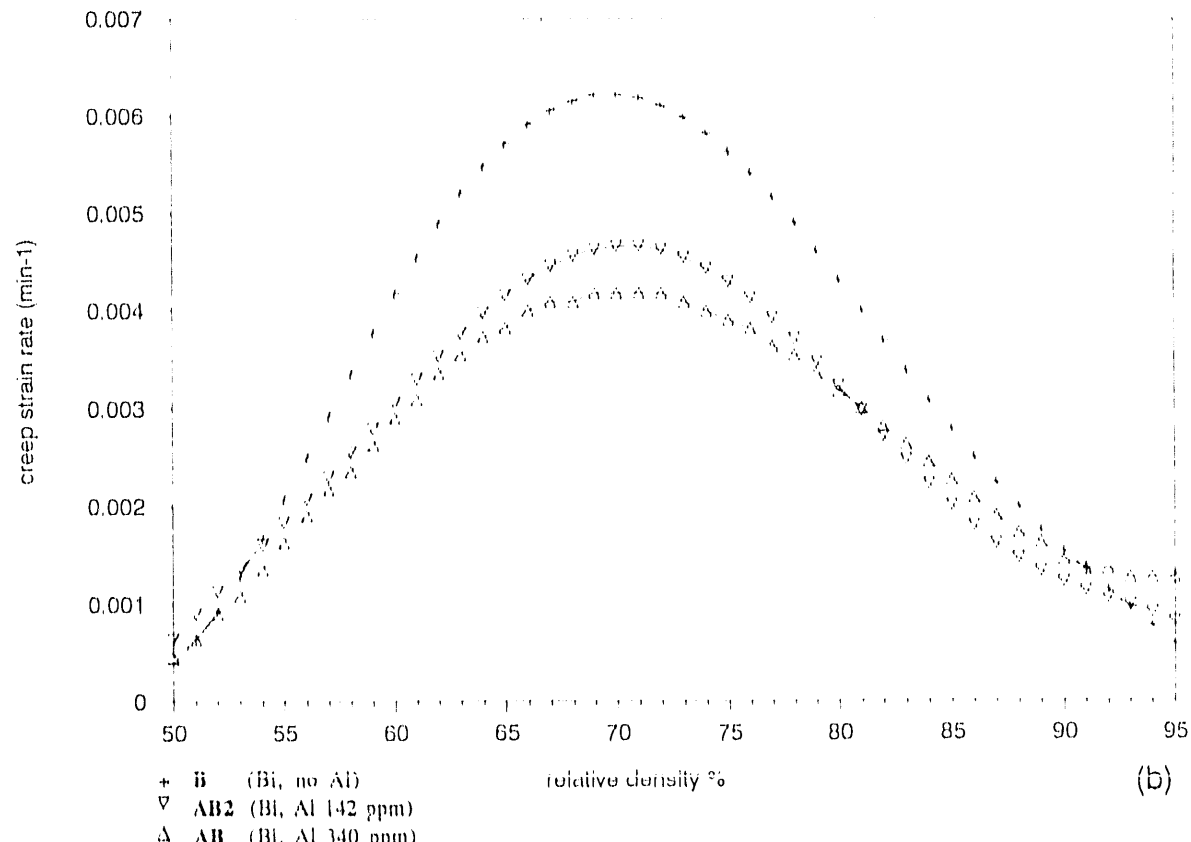

Fig. 15 RATIO BETWEEN DENS. AND CREEP RATE vs. DENSITY

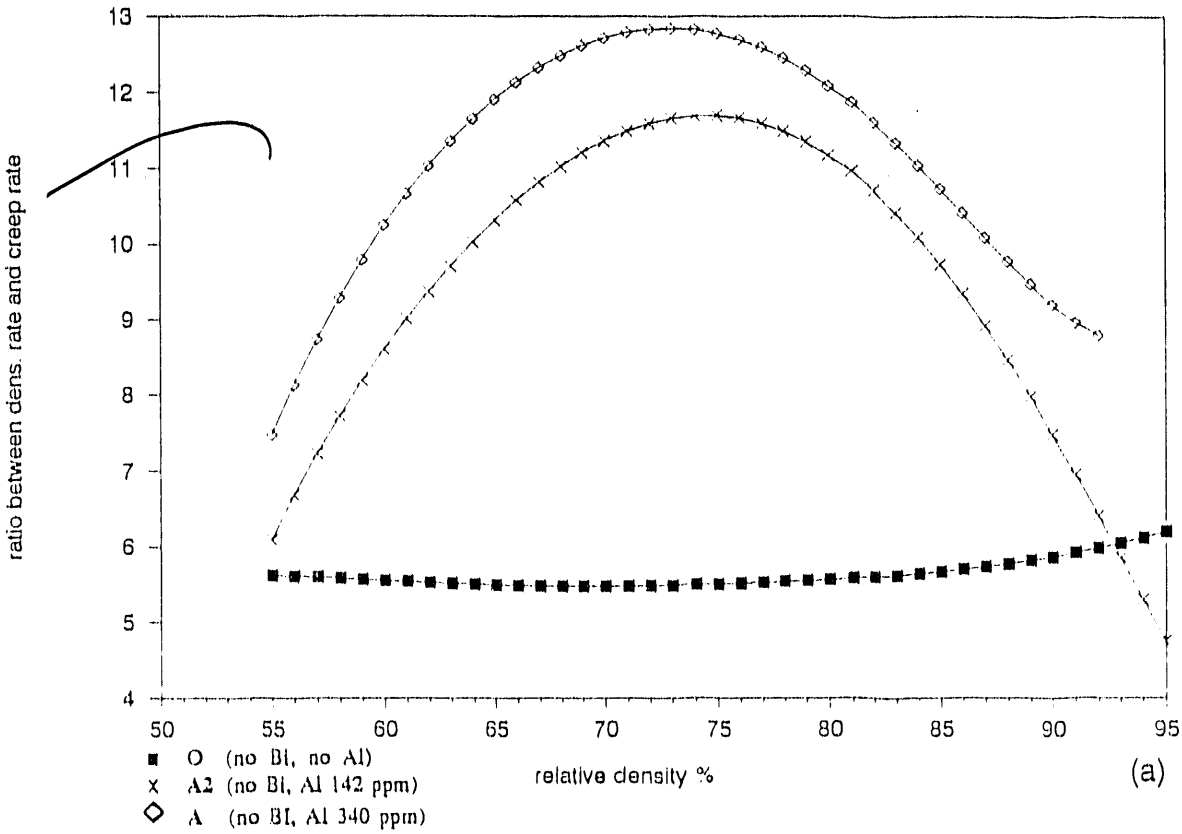

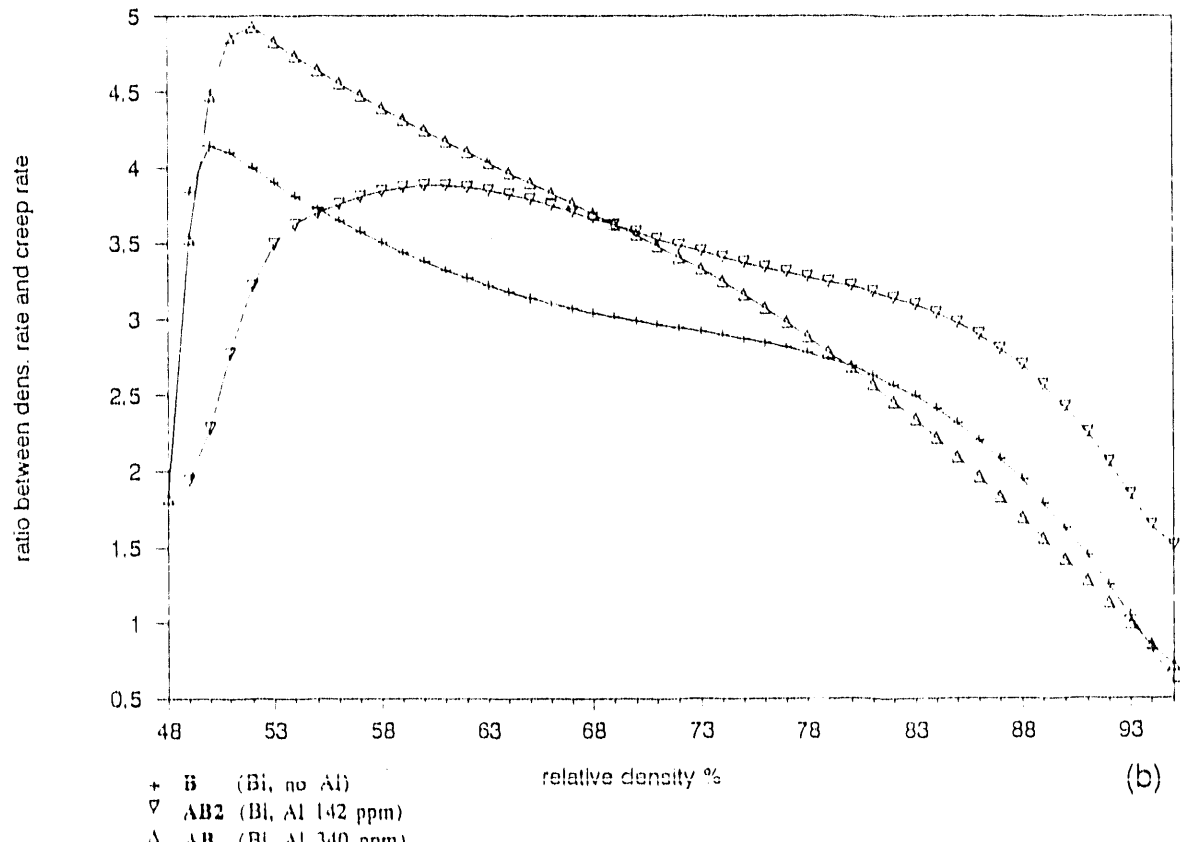

Densification rate - AB powders

Fig. 16

Effect of the green density

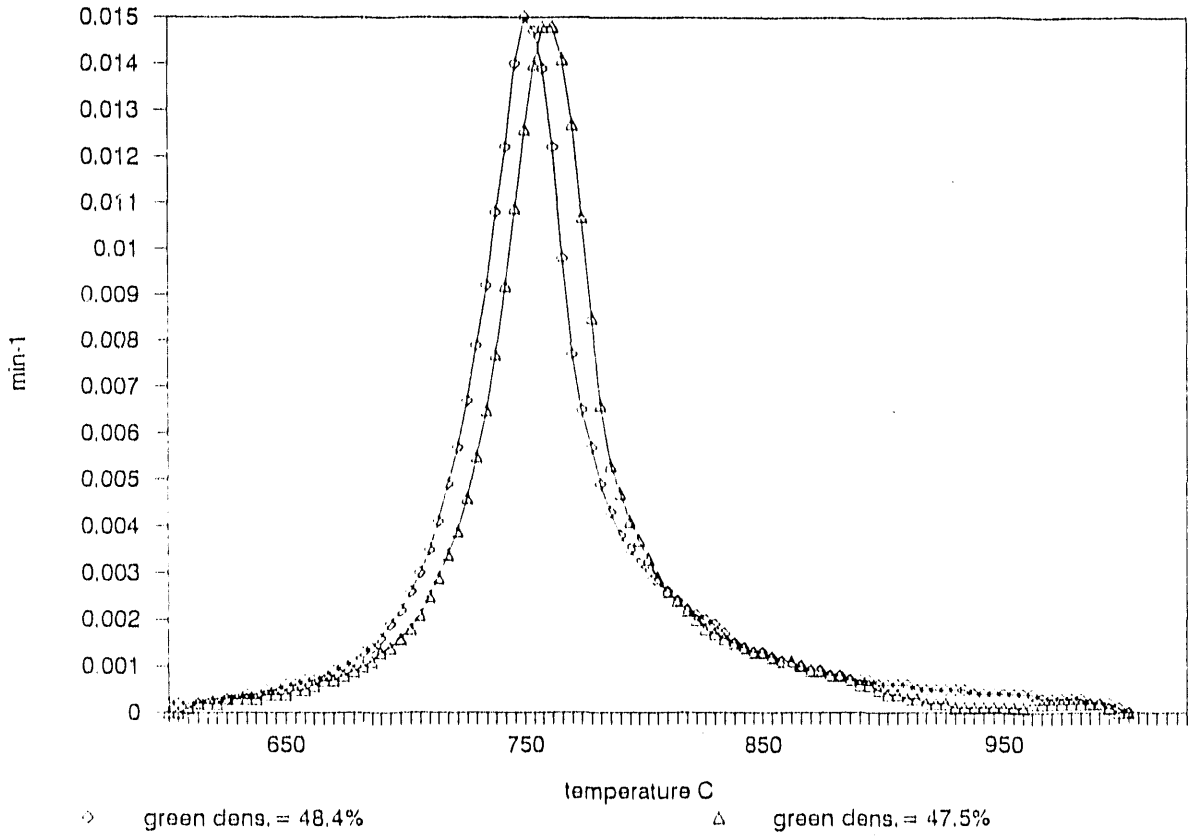

Neck region between two grains

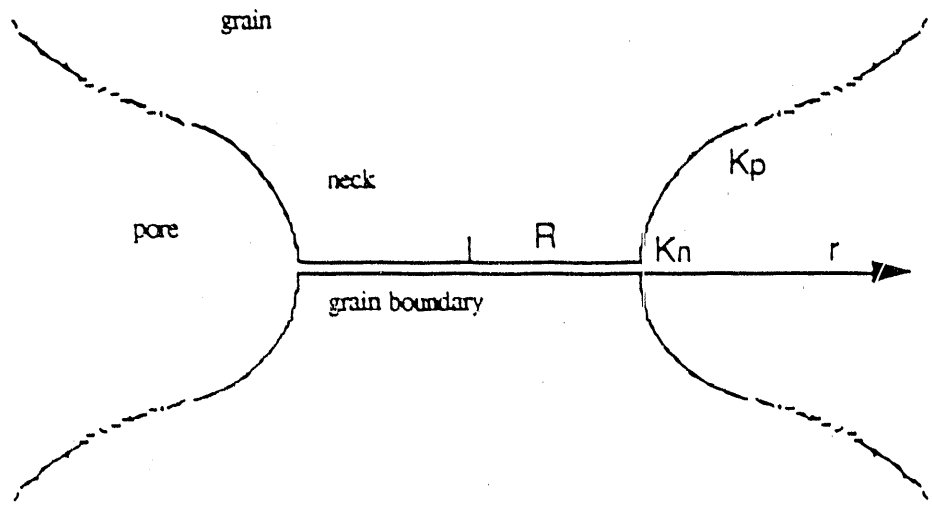

R = Neck radius

r = radial distance from the neck

Kn = pore curvature at the grain boundary - neck intersection

Kp = maximum pore curvature

Fig. 17

-END-

DATE FILMED

01 / 15 / 91